NASA TECHNICAL NOTE

NASA TN D-6492

PRELIMINARY STUDIES BY FIELD ION MICROSCOPY OF ADHESION OF PLATINUM AND GOLD TO TUNGSTEN AND IRIDIUM

by William A. Brainard and Donald H. Buckley

Lewis Research Center
Cleveland, Ohio 44135

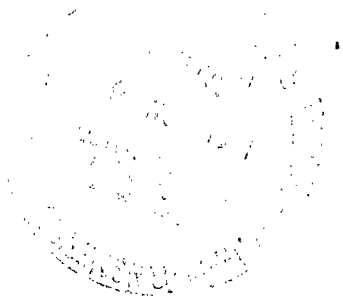

NATIONAL AERONAUTICS AND SPACE ADMINISTRATION • WASHINGTON, D. C. • OCTOBER 1971

1. Report No.	2. Government Accession No.	3. Recipient's Catalog No.
NASA TN D-6492		

4. Title and Subtitle: PRELIMINARY STUDIES BY FIELD ION MICROSCOPY OF ADHESION OF PLATINUM AND GOLD TO TUNGSTEN AND IRIDIUM

5. Report Date: October 1971

6. Performing Organization Code:

7. Author(s): William A. Brainard and Donald H. Buckley

8. Performing Organization Report No.: E-6383

9. Performing Organization Name and Address:
Lewis Research Center
National Aeronautics and Space Administration
Cleveland, Ohio 44135

10. Work Unit No.: 129-03

11. Contract or Grant No.:

12. Sponsoring Agency Name and Address:
National Aeronautics and Space Administration
Washington, D. C. 20546

13. Type of Report and Period Covered: Technical Note

14. Sponsoring Agency Code:

15. Supplementary Notes:

16. Abstract

Adhesion experiments with platinum and gold contacting tungsten and iridium field-ion-microscope emitter tips were conducted in vacuum. Platinum contacting tungsten at 300 K showed an ordered surface believed to represent mechanical transfer of the platinum onto the tungsten in an ordered manner. Gold contacting tungsten at 78 K showed essentially a random transfer with some clustering of gold atoms. Gold transferred onto iridium by contacting at 78 K presented an ordered appearance due to decoration of ledge sites by the gold atoms. Iridium contacted by platinum showed a highly ordered surface believed to be epitaxial transfer of platinum on the surface. Contacting iridium with platinum without vibration isolation caused large globs of platinum to transfer onto iridium in an ordered manner.

17. Key Words (Suggested by Author(s))		18. Distribution Statement
Field ion microscope	Tungsten	Unclassified - unlimited
Adhesion	Iridium	
Platinum	Vacuum	
Gold		

19. Security Classif. (of this report)	20. Security Classif. (of this page)	21. No. of Pages	22. Price*
Unclassified	Unclassified	56	$3.00

* For sale by the National Technical Information Service, Springfield, Virginia 22151

PRELIMINARY STUDIES BY FIELD ION MICROSCOPY OF ADHESION OF PLATINUM AND GOLD TO TUNGSTEN AND IRIDIUM

by William A. Brainard and Donald H. Buckley

Lewis Research Center

SUMMARY

Adhesion experiments with platinum and gold contacting tungsten and iridium were conducted in vacuum by using the field-ion-microscope emitter tip as part of the contacting couple. Tungsten-platinum contact in vacuum at 300 K showed an ordered surface believed to be platinum which had transferred to the tungsten surface. It was necessary to raise the voltage above the tungsten evaporation voltage to remove the platinum from the (110) region.

Tungsten-gold contacts showed a random transfer of the soft gold to the tungsten surface. Diffuse bright spots were observed following contact, which evaporated near the best-image voltage. Small clusters of atoms were observed on the (110) plane.

Iridium contacted by gold at 78 K in vacuum showed an ordered distribution of transferred gold atoms. No diffuse spots were observed. Gold atoms decorating the ledge sites gave the ordered appearance.

Platinum contacting an iridium tip caused a near-epitaxial transfer of platinum to the iridium surface. After contact, the entire surface evaporated uniformly until the last of the platinum was removed from the (100) region. A similar contact made without vibration isolation showed highly enhanced areas of platinum transferred in a glob-like manner to the surface. The glob-like transfer still appeared to have taken on the order of the substrate. This type of transfer may have resulted due to interfacial friction or cyclic stresses caused by the ambient vibrations during contact. Increasing the load, under vibration-controlled conditions, to 1.3 to 1.5 milligrams caused the shank of the tips to bend over and deformation to occur in the slip region. Even with severe loading, the general character of the contacted surface was similar to lighter load contacts.

INTRODUCTION

Fundamental work in the area of friction, adhesion, and wear puts great emphasis on the study of solid surfaces. Increased emphasis has been placed on those techniques which enable the fundamental properties of materials to be studied and more precise relationships between these fundamentals and lubrication theory to be established.

Techniques such as scanning and transmission electron microscopy, low-energy electron diffraction (LEED), Auger emission spectroscopy, and field ion microscopy (FIM) have all found usefulness in the study of solid surfaces and are being applied to lubrication research on a fundamental level.

The utility of the field ion microscope in studying adhesion was demonstrated by Müller and Nishikawa (refs. 1 to 3). This work demonstrated that the adhesion process could be studied on an atomic scale by utilizing the field emitter as one-half of an adhesive couple.

The field emitter, whose size is generally from 100 to 1000 Å in radius, can be field evaporated to give a surface that is nearly atomically clean and crystallographically perfect. This nearly perfect surface can then be contacted by another metal or nonmetal under various loads in air, in vacuum, or in the presence of a selective contaminate. After contact, the emitter can be examined on an atomic scale to determine the effects of the contact on the emitter material. Deformation can be observed by the generation of dislocations, slip bands, twins, etc.; and evidence of metallic transfer can be observed. Further, with controlled field evaporation, the specimen can be examined layer by layer into the bulk of the material to determine the extent of subsurface deformation.

The objective of this investigation was to use the field ion microscope to gain a better fundamental understanding of the process basic to friction and adhesive wear, namely adhesion. The metal combinations selected do not necessarily represent material combinations that may be encountered in practical lubrication systems. They do represent two different crystal systems, namely the body-centered cubic (bcc) and the face-centered cubic (fcc), the systems in which most materials used in lubrication components do crystallize. Therefore, understanding the adhesive behavior of these materials will lend insight into the adhesion, friction, and adhesive wear of materials presently used. A fundamental appreciation for adhesive behavior at the atomic level will aid in the selection, on a rational basis, of useful components for lubrication systems.

APPARATUS

Field Ion Microscope (FIM)

The field ion microscope is shown schematically in figure 1. The microscope is constructed of a bakeable, all-metal vacuum system equipped with metal gasket. The field emitter is tack welded to a nickel wire loop which slips over two copper posts extending down from the end of the cryogenically cooled cold finger. Also attached to the copper posts is the high-voltage (0 to 30 kV) lead. The copper-post mounting disk is separated from the metal (ground) end of the cold finger by sapphire disks which serve both as electrical insulators and thermal conductors. This cold finger design was adopted from reference 4. The cold finger is cooled by filling it with either liquid nitrogen (78 K) or liquid helium (4.2 K), or by using a two-stage commercial cryostat which can be inserted down the cold finger tube to liquify hydrogen (21 K). The cold finger is welded to a flange which mates with a bellows assembly used to vary the vertical position of the tip. Tip-to-screen distance can be varied from 8 centimeters to 5 centimeters by bellows compression.

The screen of the FIM is a tin-oxide-coated fiber optic window 7.6 centimeters in diameter with an average fiber diameter of 16 micrometers. Phosphor is coated on the inside of the fiber optic screen by utilizing an artist's airbrush. The phosphor used was a manganese-activated zinc orthosilicate. This phosphor has been shown to have reasonably good ion response coupled with a tolerable decay time (ref. 5). Photography of the field ion image is done by direct-contact photography methods. The film is pressed directly against the outside of the fiber optic window and this essentially utilizes the fiber bundles as the "lens" to transmit the image from inside the screen to the emulsion. This method of photography has been shown to reduce photographic exposure times by as much as an order of magnitude (ref. 6). The film used for photography was Tri-X Pan 4-by-5 sheet, although Polaroid type-57, 3000-speed film was also used for immediate evaluation of image quality and to establish the best-image voltage.

The imaging gas system consisted of cylinders of research-grade helium and neon which were bled into the evacuated microscope to a pressure of approximately 3 millitorr with a variable leak valve.

The vacuum system of the field ion microscope consisted of a cryosorption fore pump, a 0.02/0.4-cubic-meter-per-second (20/400-liter/sec) combination ion pump and water-cooled titanium getter pump, and a noble-gas-pumping 50-liter-per-second ion pump. Chamber pressure was monitored, at imaging pressure, by a thermocouple gage and at ultra-high-vacuum (UHV) conditions with a cold-cathode-triggered discharge gage. With moderate bakeout (250° C), chamber pressure was 10^{-10} torr.

The electrical block diagram of the FIM is shown in figure 2. A regulated, reversible, 0- to 30-kilovolt dc power supply is used in the positive mode for field ionization. A 2-nanosecond pulser with variable pulse height from 0 to 2 kilovolts is floated at the 30-kilovolt supply bias level. The pulser is capable of single manual pulsing or repetitive pulsing at 60 hertz. The pulser permits controlled field evaporation of the specimen at rates from 1 atomic layer to several layers per second. A 500-megohm resistor for preventing damaging electrical breakdowns inside the microscope is attached between the high-voltage (HV) supply and the pulser. Also floated in series is a solid-state electrometer for measuring the ion and emission current. The electrometer is protected against breakdown by an input-to-chasis diode couple (27 volts breakdown voltage).

Emitter Contactor Apparatus

The manipulator which was used for contacting the field ion emitter tip, which is a modification of a device used in reference 7, is shown schematically in figure 3. Basically the device is a stainless-steel beam mounted on a taut band. On one end of the beam is a small permanent bar magnet. Above and below the bar magnet, outside the glass vacuum tube, are two small electromagnets wired so that like poles face the permanent magnet. The beam can be made to move either up or down by varying current to the electromagnets. On the other end of the beam is a platform which moves under the field emitter tip during contact. On the platform is the material with which the tip is touched. The platform is moved horizontally to a location directly under the emitter tip or to a location exposing the emitter tip by means of the bellows shown in figure 1.

Also mounted on the beam is a stainless-steel flag which acts to intercept the light from a small lamp to a photocell. The shadow cast on the photocell changes the resistance of the cell, causing a change in voltage to the electromagnets. This photocell-electromagnet voltage system serves to damp out vibrations. The photocell voltage also serves as a monitor for beam position. Photocell voltage is amplified and read on a multirange recorder. Any change in beam position is reflected in photocell voltage which is recorded. By monitoring the time differential of the photocell voltage on a recorder with suitable amplification, the contact of the field emitter tip can be sensed by the opposite but equal force applied to the beam by the tip. The contact causes a readily observable spike on the recorder trace.

The contact of the tip was also sensed by utilizing the deflection of a thin spring. In this case a foil of the noble metal was welded to a linear spring. When contact with the field tip occurs, the spring deflects enough so the foil makes an electrical contact with an electrode just below the foil. The spring and foil are grounded, thus causing a meas-

urable current between the electrode and ground which is read on a meter outside the microscope. The gap between the foil and the electrode can be set to vary the force required to give a current indication. The gap spacing could be set close enough to allow sensing of forces of 0.25 milligram.

Precalibration of contact force as a function of electromagnet current is accomplished by the use of an electronic balance with a sensitivity of 0.01 milligram. By applying a larger electromagnet current to the top magnet, a known load can be applied to the contacted tip. After contacting and loading, the current to the top electromagnet is reduced until the tip and contact material separate.

In order to reduce the influence of ambient vibrations on the experiments, the entire field ion microscope (including pumps, power supplies, gages, gas supply system, etc.) and the emitter contactor apparatus are mounted on a vibration isolation table. The vibration table utilizes air piston suspension and has a natural frequency of 1.1 hertz with better than 90-percent isolation at resonant frequencies between 7 and 20 hertz.

PROCEDURE

The tip contact procedure is shown as a flow diagram in figure 4. The tip is electro-etched from fine high-purity wire to an extremely fine radius (<500 Å). Methods for tip preparation are discussed in the literature (ref. 8). Following etching, the specimen is mounted on the cold finger and the FIM is pumped into the UHV range.

The tip is imaged at a pressure of approximately 3 millitorr with either helium or neon gas. Field evaporation is conducted in order to increase tip radius and to prepare a nearly perfect crystallographic surface. After field evaporation, the image gas is pumped out while the high voltage is kept on to prevent contamination of the tip. The cold finger can be warmed by blowing the nitrogen (25° C) gas down the cold finger tube. After the tip is warm and the pressure is less than 10^{-9} torr, the high voltage is turned off. A clean surface can be maintained for several minutes at pressures below 10^{-9} torr.

Two procedures for contact are used; one for metals (conductors), another for nonmetals (insulators). For nonmetals, the tip contactor is moved under the tip by bellows compression. The contactor platform and contact material are then brought up by motion of the beam until they are within 0.5 millimeter of the tip as determined visually. From this point, the contact platform is slowly raised until contact is sensed. This procedure may take several hours to accomplish at the extremely slow rate of motion necessary to avoid severely damaging the field emitter tip by impacting. After the tip is in contact, a load can be applied.

For metals, a method which utilizes the emission current as a function of tip-to-

contact-material distances is used. This method makes use of the fact that the smaller the separation between the tip (cathode) and contact material (anode), the smaller the voltage necessary to maintain a constant current (ref. 9). A similar method was employed and discussed in reference 8. The conductive contact materials are at ground potential, and a negative potential of between 200 and 300 volts is applied to the tip. The contact plate is brought toward the tip until an emission current of 5×10^{-9} ampere is read. For a clean tungsten tip of 500 Å radius, a current of 5×10^{-9} ampere indicates a tip-to-contact-material distance of 2000 Å (ref. 6). After the emission current is established, the negative voltage is turned off and the same contact procedure is carried out as for nonmetals, except that the tip is so close that only minutes are needed to make contact.

After contact and loading, the tip and platform are unloaded and the contact platform is moved back. The tip is then imaged again to establish the effects of adhesion on the emitter tip. Controlled field evaporation of the tip materials will permit monolayer-by-monolayer examination of the tip and thus, to a limited extent, bulk effects of the adhesive contact.

FIELD ION MICROSCOPY

Background

The field ion microscope was developed from its forerunner, the field emission microscope. Field emission is the tunneling of electrons from a metal surface at field strengths of the order of 10^7 volts per centimeter. Emission is a consequence of the reduction of the surface potential barrier by the applied field. The current density for field emission is expressed by the Fowler-Nordheim equation (ref. 10)

$$J = 6.2\times10^{-6}\,\frac{(\mu/\varphi)^{1/2}}{\alpha^2(\mu+\varphi)}\,F^2\exp\left(-6.8\times10^{7}\,\varphi^{3/2}\,\frac{\alpha}{F}\right)$$

where

J current density, A/cm^2

μ Fermi energy relative to bottom of conduction band, eV

φ work function, eV

F field strength, V/cm

α function of F and φ (generally between 0.8 and 0.9)

The field emission microscope, however, is limited to a resolution of about 25 Å by the tangential velocity of the emitted electrons and by their De Broglie wavelength (ref. 8). This limited resolution led to the use of positive ions for imaging, rather than electrons, with an obtainable resolution of between 2 and 3 Å.

Image formation with positive ions rather than electrons required field strengths an order of magnitude above those for field emission. For helium ion imaging, the field strength needed for ionization is 4.4×10^8 volts per centimeter (ref. 8). To obtain these high fields, it is necessary to use extremely small sharp tips, generally less than 1000 Å in radius. The field strength at the emitter tip is given by the expression (ref. 10)

$$F = \frac{V}{kR}$$

where

F field strength, V/cm

V voltage, V

R radius of tip, cm

k geometric constant (~5)

Thus for tips with a radius of 1000 Å (10^{-5} cm), voltages of the order of 22 000 volts are needed for helium ion imaging. For a tip with a larger radius (e.g., 10^{-3} cm), the voltage necessary for imaging would be prohibitively high.

These high fields required for ion image formation place severe restrictions on emitter materials. A mechanical stress is imposed on the tip by the applied field. The stress, given by $F^2/8\pi$, at the helium image field is of the order of 10^6 newtons per square centimeter (10^{11} dynes/cm^2).

This imposed stress is one of the basic limitations of field ion microscopy and generally limits those materials that can be reliably imaged in the helium field ion microscope to the refractory metals.

Image Formation

The formation of a field ion image is a process whereby a neutral image-gas atom is ionized in the vicinity of the field emitter tip by the extremely high field. The field ionization process is discussed in detail in several references (refs. 8, and 10 to 14). Ionization of a neutral gas atom occurs when tunneling of an electron from the gas atom into the positive tip takes place. The probability for tunneling becomes appreciable

only at the high electric field required for image formation. At these high fields (10^8 V/cm), the electron potential barrier is reduced to a width comparable to the De Broglie wavelength of the electron (ref. 8).

Figure 5 shows schematically the field ionization-image formation process. Ionization occurs at some distance above the tip surface; for helium ionization the critical distance above the surface is about 4 Å (ref. 8).

It was realized early in the development of the FIM that cooling the emitter tip resulted in increased resolution by accommodating the imaging gas molecules at the tip temperature, thus decreasing their kinetic energy (ref. 13). Theoretical considerations show that for a 1000-Å radius tip, resolution increases from more than 15 Å at 1630 K to 3 Å at 21 K (ref. 8).

Field Evaporation

Field evaporation is a process whereby metal atoms from the tip are removed in the form of positive ions. It is a field-dependent process, requiring field strengths above the helium image field for most of the refractory materials. For example, the observed field for which tungsten evaporates is 5.7×10^8 volts per centimeter; whereas, for imaging, the field is 4.4×10^8 volts per centimeter (ref. 10). Some materials evaporate at field strengths below that for helium ion imaging, thus a stable image of these materials cannot be obtained with helium as the image gas.

Field evaporation is the method that provides a near-perfect surface and without which field ion microscopy would not be the useful tool it is. In tip preparation, the process is self-regulating in that sharp asperities and edges preferentially evaporate because of local field enhancements at these points until a smooth surface is obtained (ref. 8). The process of field evaporation is discussed in depth in references 8 and 10.

Image Interpretation

The interpretation of field ion micrographs requires considerable care. The identification of defects is not always straightforward. An accurate interpretation of a micrograph requires an accurate knowledge of the geometry of the surface, the interaction of the defect with the surfaces, and the mechanism of the image formation itself. Considerable progress in the interpretation of defects in field ion images has been made through the use of computer simulation. An in-depth discussion of the interpretation of field ion micrographs is available in the literature (refs. 8, 10, and 15 to 26).

In order to isolate changes occurring on the metal surface from causes other than

adhesive contact, a series of noncontacting tests were run. It has been shown by several investigators that strain release due to the removal of the field-induced stress and reaction of the tip with the residual gas phase can significantly alter the atomic structure (refs. 8, and 27 to 30). Tests were run with the same field-off time and pressure conditions that would occur during adhesive contact.

Before-and-after micrographs were compared with a two-color superposition technique described in reference 13. With this technique, the before-and-after black-and-white micrographs are photographed on the same color plate by superimposing one on the other. The before black-and-white micrograph is photographed with a green filter (Wratten No. 58) and the after black-and-white micrograph is then photographed with a red filter (Wratten No. 25). Any spot which is photographed in both red and green will process as yellow. A spot which appears only in the first micrograph will appear green. Similarly, a spot appearing only in the second micrograph appears red. Thus, green spots indicate where surface atoms have been lost, red spots where new atoms appear, and yellow spots where there has been no change.

Figure 6 shows the two black-and-white micrographs for a tungsten tip before and after being exposed to the residual gases at zero field for 60 minutes. Figure 7 shows the color superposition print of the micrographs in figures 6(a) and (b). The changes observed are minimal; only a few green spots are observed, indicating very little corrosive attack. Further, equally few red spots are visible. This means that if comparable zero field times are used at equivalent background pressures for the actual adhesive contact with tungsten, the changes observed will be primarily due to the interaction of the adhesive couple.

Figure 8 shows a color superposition for tungsten after an exposure twice that shown in figure 7 (4.2×10^{-6} torr-sec against 2.1×10^{-6} torr-sec); the changes observed are considerably more pronounced. The tip in figure 8 was kept at 78 K during the field-off time; however, reference 28 indicates that corrosion of tungsten by the predominate residual gases occurs even at 21 K.

Figure 9 presents two black-and-white micrographs of iridium before and after a zero field exposure for 60 minutes at 2×10^{-10} torr. Figure 10 shows the color superposition print. Surface changes again are minimal. However, it is of interest to note the almost complete loss of atoms making up the "zone decorations" which crisscross on the (001) plane steps. This is probably a more potentially reactive area due to partially occupied orbitals of those atoms which make up the decorations (ref. 31).

RESULTS AND DISCUSSION

The elemental metals tungsten and irridium were chosen for this investigation be-

cause they image reliably in the field ion microscope, and as mentioned earlier, exhibit stability under conditions which exist during actual experimentation. Further, they exhibit the body-centered-cubic and face-centered-cubic crystal structure types, respectively. The stereographic projections for these crystal types are given in the appendix.

Tungsten-Platinum

Figure 11(a) presents a field ion micrograph of a tungsten tip prior to contact. The tip radius is approximately 480 Å. Figure 11(b) shows a micrograph of the same tip after contact with platinum at 300 K in vacuum. The micrograph in figure 11(b) was taken at a voltage 2000 volts below the precontact micrograph.

Several immediate observations can be made. First, there is considerable disorder characterized by many random bright spots. Second, the character of several planes has changed. For example, on (211) the inner ring has decreased in diameter and is considerably disordered on the plane edge. Further, note the variations in brightness. The (111) plane shows deviation from the normal (111) packing. The higher index planes are completely obscured.

In order to interpret these results, it is helpful to discuss vapor deposition studies of metals on tungsten as well as LEED and Auger emission spectroscopy studies of noble metal adhesion. The LEED studies showed that the noble metals gold and silver, when brought into mechanical contact with bcc iron, transferred to the iron in an ordered manner even though the noble metals were not cleaned other than by vacuum bakeout. Further, the LEED-Auger studies have shown that transfer of metals during adhesion can be correlated to cohesive energy data.

The metal with the lowest cohesive energy will transfer to the metal with the higher cohesive energy during solid-state contact (ref. 32). The cohesive energies for tungsten and platinum are 836 and 564 kilojoules per gram-atom (200 and 135 kcal/g-atom), respectively (ref. 33). Thus, during solid-state contact it is expected that platinum will transfer to the tungsten surface.

Vapor deposition studies of nickel on tungsten (ref. 34) and platinum on tungsten (refs. 34 and 35) have shown that the deposited films show a high degree of order. More specifically, nickel deposited on tungsten at ~118 K exhibited a high degree of order, while nickel deposited at 300 K formed a perfect ordered layer even showing the "zone decorations" characteristic of the tungsten surface. For platinum on tungsten, appreciable ordering occurs at 100 to 200 K (ref. 35); while the initial deposition of platinum on tungsten below 250 K was observed in reference 36 to cause growth of platinum islands, particularly on the (111) and (100) planes.

In view of the preceding discussion, it might therefore be expected that platinum will transfer to the tungsten surface during adhesive contact and that platinum would tend to order on the tungsten. It must be realized, however, that the platinum in a mechanical-contact situation arrives at the surface with less mobility than vapor-deposited platinum atoms; the transferring platinum adheres to the tungsten as clusters which have been pulled out of the platinum matrix.

It is believed that the micrographs after contact show a platinum layer that is partially ordered on the tungsten substrate. Comparing the planes (111), (211), and (310) in figures 11(a) and (b) shows a marked difference which represents the change from an ordered tungsten surface to a platinum surface. On the (211) plane a considerable variation in spot brightness is evident, the brighter spots being platinum atoms in adatom positions.

Raising the voltage to 14.5 kilovolts (fig. 11(c)) causes several bright spots to desorb (e.g., on the (110) and (310) planes), as well as other bright spots to appear on the ledges surrounding the (110) plane. Further, increasing the voltage to 15.0 kilovolts (fig. 11(d)) causes similar results. At 15.5 kilovolts (fig. 11(e)) a general blurring in the low-work-function regions (121), (111), and (211), etc., indicates the onset of field evaporation. At 16.0 kilovolts (fig. 11(f)), the blurring is more pronounced. The ledges around the (110) plane are readily visible. The irregular brightness of the image spots making up these rings around (110) suggest irregular packing with many vacancies and adatoms at the ledge sites.

The precontact image was taken at 16.0 kilovolts, thus for helium best-image voltage the electric field was $\sim 4.4 \times 10^8$ volts per centimeter. This field strength is too low for tungsten evaporation (5.7×10^8 V/cm). Platinum, however, field evaporates at 4.7×10^8 volts per centimeter (ref. 8); thus the onset of evaporation for the contacted surface, if covered with platinum, is in close agreement with the platinum evaporation field.

Figure 11(g) presents a micrograph of the same surface after raising the voltage above 16.0 kilovolts for a few seconds. The low-work-function regions have been stripped of the platinum and resume their normal appearance. The regions around (110), however, are still disordered although many ledge-site bright spots have desorbed. Further evaporation (fig. 11(h)) shows a decrease in the diameter of the remaining platinum film as it evaporates from the edges inward. This sequence of evaporation to an increasingly smaller diameter of film was observed for nickel on tungsten (ref. 34). The authors of reference 37 vapor deposited platinum on tungsten and found it necessary to evaporate the underlying tungsten before removing all the platinum from the (110) planes and ledges. In this reference the authors calculated the binding energy for platinum on various tungsten planes from desorption data and found it to be the highest on the (110) plane.

The final micrograph of this series (fig. 11(i)) shows the tungsten surface after complete removal of all the remaining platinum. The final micrograph was taken after the tip voltage had been raised for a few seconds above the previously determined tungsten evaporation field by approximately 10 percent. The tungsten substrate is perfectly ordered and no deformation is observed.

Tungsten-Gold

Figure 12(a) is the precontact micrograph of a tungsten tip of approximately 350 Å radius. Figure 12(b) shows a micrograph taken at 2000 volts below the precontact image, immediately after gold-tungsten contact. In this case, the tip was kept at 78 K during the contact. Reference 38 demonstrated by vapor deposition of gold on tungsten surfaces that gold deposits can be seen by helium field ion microscopy and that gold is stable with regard to field evaporation to 80 to 97 percent of the tungsten evaporation field. These authors further find no ordering of gold deposited on tungsten at low temperatures and that heating to 800 K or higher was necessary for ordering. Figure 12(c) shows the tip when brought up to the precontact image voltage. Several diffuse spots are present on the surface which were sharp and bright at 11.0 kilovolts. The arrows in figures 12(b) and (c) shows how these spots grow diffuse with increasing voltage. It is not clear what these diffuse spots represent, they may be clusters of several gold atoms approaching the field evaporation threshold. The only order evident in figure 12(c) is the (110) plane and surrounding ledges, which are believed to be the underlying tungsten substrate.

Raising the voltage to 14.5 kilovolts for 30 seconds causes desorption of most of the diffuse spots, revealing more of the underlying tungsten. It is of particular interest to note the resolution on the (110) plane in figure 12(d). Individual clusters can be resolved. This enhanced resolution suggests the clusters are sitting on top of the (110) plane rather than in the plane.

Figure 12(c) was taken after further increasing the voltage to 15.5 kilovolts for 30 seconds. Evaporation has occurred at all points on the surface (note the decrease in the diameter at the (110)). Figure 12(f) was taken after still further evaporation. The cluster in the near center of the (110) plane is now visible as the (110) plane collapses. Further increasing the voltage to 16.25 kilovolts for 5 seconds completely cleans the remainder of the tip.

The gold-tungsten contact represents the situation where the softer gold transfers to the tungsten but assumes no specific crystallinity; rather it is fairly randomly distributed with some apparent clustering of the gold atoms.

Iridium-Gold

Figure 13(a) shows the micrograph for an iridium tip prior to contact. Figure 13(b) is the iridium immediately after contact with gold in vacuum. The iridium tip was held at 78 K during the contact. There is some evidence of order of the transferred gold atoms. Note particularly the rings extending around the (111) plane and the partial rings around the (100) plane. In figure 13(c) the order around the (100) plane is more apparent. Note the absence of bright diffuse spots, which were apparent after tungsten-gold contact. Raising the voltage to the original iridium field evaporation voltage for 30 seconds causes further desorption of gold as well as some evaporation of the underlying iridium substrate. It is of particular interest to observe the ledges around (111), noticing the bright spots randomly spaced along the ledges with the fainter iridium atoms imaging underneath (fig. 13(d)). It is believed these bright spots are gold atoms found along the ledge sites. Figure 13(e) presents the final micrograph after field evaporation at 15.2 kilovolts for 30 seconds. Most of the surface is now ordered iridium, with the exception of part of the (111) and the (100) plane and a few surrounding ledges. This micrograph is very similar to a gold-iridium contact FIM micrograph published in reference 39.

Iridium-Platinum

The final series of contacts were made with platinum contacting an iridium tip. It is known from vapor deposition studies that platinum forms epitaxially on iridium at temperatures as low as 200 K (ref. 40). The cohesive energy of iridium at the standard state (298 K) is 664 kilojoules per gram-atom (159 kcal/g-atom) (ref. 33), thus higher than that of platinum at 564 kilojoules per gram-atom (135 kcal/g-atom). Therefore, transfer ought to occur from platinum to iridium.

Figure 14(a) is a micrograph of iridium prior to contact. It shows a somewhat imperfect tip with a grain boundary and nonimaging furrows. Figure 14(b) is the micrograph taken immediately after platinum contact with the tip at 78 K, a load of approximately 0.5 milligram, and a voltage of 18.0 kilovolts. The surface has a fairly high degree of order and is characterized by a dark nonimaging area between the (100) plane and the (311) plane. Figure 14(c) shows the same surface after the voltage was raised to 19.0 kilovolts. (The precontact image was taken at 20.0 kV.) Figure 14(c) indicates that evaporation has occurred over the entire surface as a consequence of the voltage increase. Further increasing the voltage to 20.0 kilovolts (fig. 14(d)) showed similar results. It is of interest to note that although the entire surface has been evaporated through at least two atomic layers, the micrograph still presents an image essentially

the same as that of figure 14(b). The dark area between the (100) and (311) planes shows very faint rings which may be the intrinsic iridium surface in a region where platinum has not covered the surface for some reason (perhaps contamination occurred at this point, preventing metal-to-metal contact). The iridium tip prior to contact was evaporated at 22.5 kilovolts; thus the increase in voltage from figure 14(b) to figure 14(d) is not sufficient to evaporate iridium although platinum evaporates from platinum at a field strength approximately 12 percent less than iridium (ref. 8). Since field is directly proportional to voltage, it is expected that for platinum on the surface, evaporation could occur at voltages below the precontact image voltage.

Figure 14(e) is a micrograph taken after raising the voltage to 22.0 kilovolts for 30 seconds. Almost perfect order is evident except in the (100) region. The dark nonimaging area is still present. Evaporating two (100) layers produced a nearly perfect surface with the exception of the nonimaging area. The characteristic iridium zone decorations also reappeared (fig. 14(f)). Since the work on vapor deposition described in reference 40 showed no evidence for zone decorations with platinum films on iridium, it thus is assumed that the micrograph in figure 14(f) represents the nearly completely cleaned iridium surface. The platinum was removed from the surface in a manner identical to that described by the authors of reference 40. The dark nonimaging area is apparently covered by some nonidentifiable contaminant and it was necessary to evaporate through five more (100) layers to remove it.

Repeating the experiments with platinum contacting iridium under the same conditions showed similar results, except that no dark nonimaging area was observed.

One experiment was conducted during which the vibration isolation table was not pressurized. The iridium tip was the same tip shown in the series in figure 14 having been completely cleaned of platinum. A micrograph of the iridium after platinum contact is shown in figure 15. It was taken after considerable field evaporation of what are believed to be large globs of transferred platinum onto the surface. These areas were particularly bright, and exposure times were reduced by a factor of 10 in order to photograph them. The marked contrast between the platinum-iridium contact with and without vibration isolation may be due to either frictional forces or cycle stress forces occurring during that contact caused by the vibration.

It is significant that even though the transfer in the latter case occurred in a glob-like manner, the transferred material appears to have taken on the ordering of the iridium surface. Note particularly where the substrate (311) and (100) planes were located.

In order to see if the apparent glob-like transfer of platinum would occur by increasing the load but sill controlling vibration, an experiment was run in which an iridium tip was contacted by platinum under a load nearly three times that used in previous vibration-controlled experiments. Figure 16 presents the results. In this case,

the precontact micrograph was centered on the (100) plane. Contacting the tip by platinum under a load of 1.3 to 1.5 milligrams caused the shank of the tip to bend so the post-contact image was displaced on the screen. Figure 17 is a magnified photograph of the iridium tip after it was removed from the microscope. The micrograph of the contacted tip looks similar to the lighter loaded platinum contact as far over as the [110] planes. There is no obvious deformation in this area. The (111) plane and ledges around it are deformed. This is expected since the primary deformation mode for fcc metals is slip on the (111) planes in ⟨110⟩ directions (ref. 41). Since this area could not be seen in the precontact micrograph, interpretation is hampered. It appears, however, that the diffuse area to the right of (111) is a slip boundary with the (001) plane (zone decorated area) being considerably displaced.

SUMMARY OF RESULTS

Adhesive experiments with platinum and gold contacting tungsten and iridium were conducted in vacuum by utilizing the field-ion-microscope emitter tip as part of the contacting couple. The following results were obtained:

Tungsten-Metal Contacts

1. Tungsten contacted with platinum in vacuum at 300 K showed an ordered surface believed to be platinum which had transferred to the tungsten surface. The platinum evaporated first from the low-work-function regions at slightly above the best-image voltage. It was necessary to raise the voltage 10 percent above the original tungsten evaporation voltage to remove the remaining platinum from the region around the (110) plane.

2. Tungsten contacted with gold in vacuum at 78 K showed essentially a random transfer of the gold to the tungsten. The post-contact micrographs were characterized by several diffuse spots which field evaporated at slightly above the best-image voltage. Small clusters of transferred atoms were observed on the (110) plane. Upon field evaporation, gold was removed from (110) and surrounding ledges last.

Iridium-Metal Contacts

1. Iridium contacted with gold in vacuum at 78 K showed an ordered distribution of the transferred gold atoms. No diffuse spots were observed. Bright spots believed to

be transferred gold atoms were observed decorating the ledge sites. These bright spots at the ledge sites were field evaporated, exposing the intrinsic iridium surface structure. The gold, during field evaporation, was removed from the (100) plane last.

2. Iridium contacted with platinum in vacuum at 78 K showed a fairly ordered surface believed to be the platinum assuming the surface structure in a near-epitaxial manner. The entire surface field evaporated through at least two layers as the voltage was raised to the precontact best-image voltage. The platinum, during field evaporation, was removed from the (100) region last.

3. Iridium contacted with platinum without vibration isolation showed highly enhanced areas of platinum transferred in a glob-like manner to the iridium surface. These transferred globs appeared to have taken on the order of the substrate structure. The transfer in a glob-like manner may have occurred as a result of interfacial friction or cyclic stress induced by the vibration during contact.

4. An iridium tip contacted with platinum under a load of 1.3 to 1.5 milligrams was bent over, yet still imaged with the (100) plane being displaced off the screen. The contacted region had an appearance similar to those obtained at lighter loads. Extensive deformation was observed in the (111) region.

Lewis Research Center,
National Aeronautics and Space Administration,
Cleveland, Ohio, June 15, 1971,
114-03.

APPENDIX - STEREOGRAPHIC PROJECTION OF BODY-CENTERED-CUBIC AND FACE-CENTERED-CUBIC LATTICES

The sterographic projections are taken from reference 8.

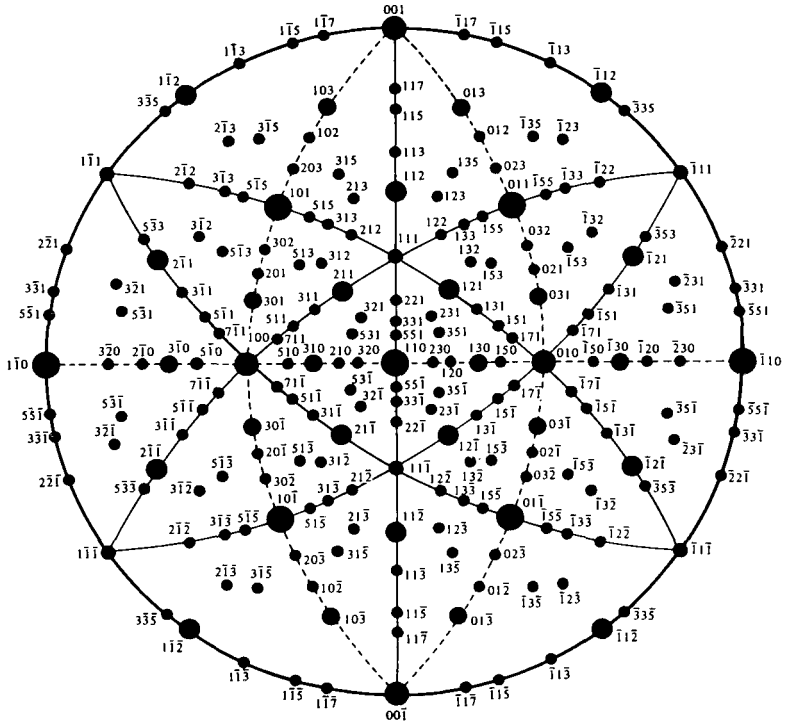

Stereographic projection of the bcc lattice; (110) oriented

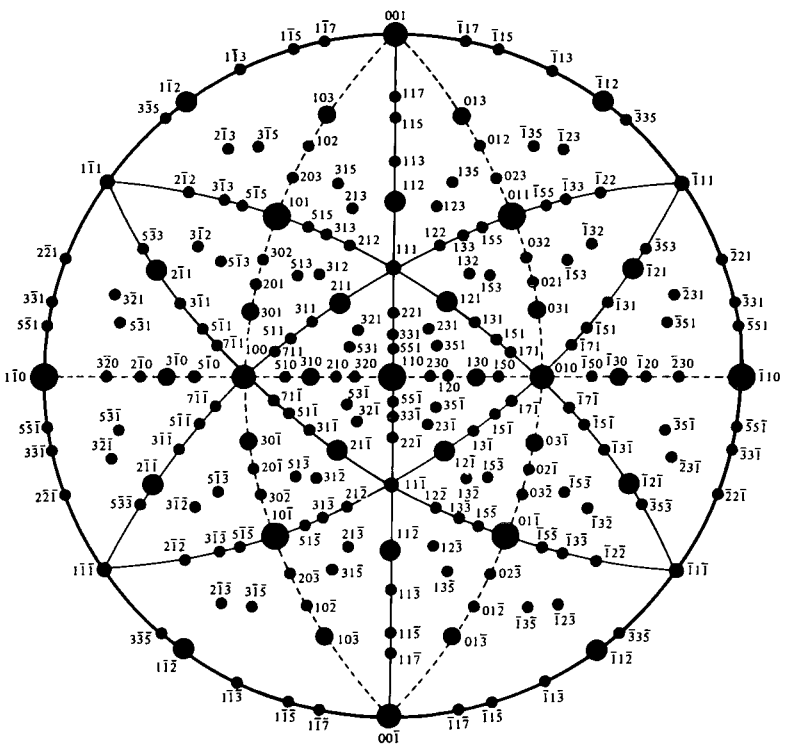

Stereographic projection of the bcc lattice; (110) oriented

REFERENCES

1. Müller, E. W.; and Nishikawa, O.: Atomic Surface Structure of the Common Transition Metals and the Effect of Adhesion As Seen By Field Ion Microscopy. Adhesion or Cold Welding of Materials in Space Environments. Spec. Tech. Publ. 431, ASTM, 1967, pp. 67-87.

2. Nishikawa, O.; and Müller, E. W.: Field Ion Microscopy of Contacts. Paper presented at the Holm Seminar on Electric Contact Phenomena, Chicago, Ill., Nov. 1968.

3. Müller, E. W.; and Nishikawa, O.: Field Ion Microscopy of Metal Contacts. Proceedings of the Engineering Seminar on Electrical Contact Phenomena, Illinois Inst. Techn., Chicago, Ill., Nov. 1967, pp. 181-193.

4. Jenkins, D. A.; Son, U. T.; Aiduck, C.; Staltz, D.; and Hren, J. J.: Advances in Experimental Field Ion Microscopy. Paper presented at 16th Field Emission Symposium, Pittsburgh, Pa., Sept. 8-12, 1969.

5. McLane, S. B., Jr.; and Müller, E. W.: A Versatile Field Ion Microscope. Tech. Rep., Pennsylvania State University, Dec. 1962.

6. Hren, J. J.; and Newman, R. W.: Fiber Optics in Field Ion Microscopy. Rev. Sci. Inst., vol. 38, no. 7, July 1967, pp. 869-870.

7. Buckley, Donald H.: Effect of Sulfur, Oxygen, and Hydrogen Sulfide Surface Films on the Adhesion of Clean Iron. NASA TN D-5689, 1970.

8. Müller, Erwin W.; and Tsong, T. T.: Field Ion Microscopy - Principles and Applications. American Elsevier, 1969.

9. Young, Russell D.: Field Emission Ultramicrometer. Rev. Sci. Inst., vol. 37, no. 3, Mar. 1966, pp. 275-278.

10. Hren, John J.; and Ranganathan, S., eds.: Field-Ion Microscopy. Plenum Press, 1968.

11. Müller, E. W.; Nakamura, S.; Nishikawa, O.; and McLane, S. B.: Gas-Surface Interactions and Field-Ion Microscopy of Nonrefractory Metals. J. Appl. Phys., vol. 36, no. 8, Aug. 1965, pp. 2496-2503.

12. Gomer, Robert: Field Emission and Field Ionization. Harvard University Press, 1961.

13. Müller, Erwin W.: Study of Atomic Structure of Metal Surfaces in the Field Ion Microscope. J. Appl. Phys., vol. 28, no. 1, Jan. 1957, pp. 1-6.

14. Müller, E. W.: Field Ion Microscopy. Science, vol. 149, no. 3684, Aug. 1965, pp. 591-601.

15. Brandon, D. G.; Wald, M.; Southon, M. J.; and Ralph, B.: The Application of Field Ion Microscopy to the Study of Lattice Defects. J. Phys. Soc. Japan, vol. 18, Suppl. II, 1963, pp. 324-332.

16. Moore, A. J. W.: Computer Simulation of Field Ion Emission Patterns of Solid Solution Alloys. Phil. Mag., vol. 16, no. 142, Oct. 1967, pp. 739-747.

17. Ranganathan, S.; Lyon, H. B.; and Thomas, G.: Computer Simulation of Field-Ion Images of Hexagonal Structures and Superlattices. J. Appl. Phys., vol. 38, no. 13, Dec. 1967, pp. 4957-4965.

18. Moore, A. J. W.; and Ranganathan, S.: The Interpretation of Field Ion Images. Phil. Mag., vol. 16, no. 142, Oct. 1967, pp. 723-737.

19. Moore, A. J. W.: The Structure of Atomically Smooth Spherical Surfaces. J. Phys. Chem. Solids, vol. 23, 1962, pp. 907-912.

20. Brandon, D. G.; Ralph, B.; Ranganathan, S.; and Wald, M. S.: A Field Ion Microscope Study of Atomic Configuration at Grain Boundaries. Acta Met., vol. 12, no. 7, July 1964, pp. 813-821.

21. Sanwald, R. C.; Ranganathan, S.; and Hren, J. J.: Computer-Simulated Ion-Emission Images of Dislocations: Screw Dislocation at the Center of {420}. Appl. Phys. Letters, vol. 9, no. 11, Dec. 1, 1966, pp. 393-394.

22. Sanwald, R. C.; and Hren, J. J.: Interpretation of Defects in Field Ion Images: fcc Materials. Surface Sci., vol. 9, 1968, pp. 257-267.

23. Perry, A. J.; and Brandon, D. G.: Computer Simulation of Spherical Crystal Surfaces: Stacking Faults and Partial Dislocation in F. C. C. Crystals. Phil. Mag., vol. 18, no. 152, Aug. 1968, pp. 353-359.

24. Brandon, D. G.; and Perry, A. J.: Computer Analysis of Dislocated Spherical Crystal Surfaces. Phil. Mag., vol. 16, no. 139, July 1967, pp. 131-140.

25. Perry, A. J.; and Brandon, D. G.: Computer Simulation of Spherical Crystal Surfaces: Dislocation Loops and Dipoles in B. C. C. and F. C. C. Crystals. Phil. Mag., vol. 17, no. 146, Feb. 1968, pp. 255-262.

26. Brandon, D. G.; and Perry, A. J.: Computer Interpretation of Lattice Defects in Field-Ion Micrographs. Surface Sci., vol. 12, 1968, pp. 461-468.

27. Nakamura, Shogo; and Müller, Erwin W.: Initial Oxidation of Tantalum Observed in a Field Ion Microscope. J. Appl. Phys., vol. 36, no. 11, Nov. 1965, pp. 3634-3641.

28. Mulson, J. F.; and Müller, E. W.: Corrosion of Tungsten and Iridium by Field Desorption of Nitrogen and Carbon Monoxide. J. Chem. Phys., vol. 38, no. 11, June 1, 1963, pp. 2615-2619.

29. Ehrlich, Gert; and Hudda, F. G.: Direct Observation of Individual Adatoms: Nitrogen on Tungsten. J. Chem. Phys., vol. 36, no. 12, June 15, 1962, pp. 3233-3247.

30. Brenner, S. S.; and McKinney, J. T.: FIM Atom Probe Analysis of Individual Image Spots Caused by Gas Adsorption. Surface Sci., vol. 20, 1970, pp. 411-416.

31. Knor, Zlatko; and Müller, Erwin W.: A Refined Model of the Metal Surface and Its Interaction With Gases in the Field Ion Microscope. Surface Sci., vol. 10, 1968, pp. 21-31.

32. Buckley, Donald H.: Adhesion of Various Metals to a Clean Iron (011) Surface Studied with LEED and Auger Emission Spectroscopy. NASA TN D-7018, 1971.

33. Seitz, Frederick; and Turnbull, David, eds.: Solid State Physics. Vol. 16. Academic Press, 1965.

34. Jones, J. P.: Arrangement of Atoms in the First Monolayer of Nickel on Tungsten. Nature, vol. 211, no. 5048, Aug. 6, 1966, pp. 479-481.

35. Naumovets, A. G.; and Fedorus, A. G.: Investigation of the Structure and Work Function of Platinum Films on Tungsten and Adsorption of Cesium on Such Films. Soviet Phys. -Solid State, vol. 10, no. 3, Sept. 1968, pp. 627-633.

36. Sugato, E.; Ishii, S.; and Masui, K.: Initial Growth of Platinum Crystals on the Tungsten Surface as Observed by the Field-Ion Microscope. Surface Sci., vol. 24, 1971, pp. 612-624.

37. Plummer, E. W.; and Rhodin, T. N.: Atomic Binding of Transition Metals on Clean Single-Crystal Tungsten Surfaces. J. Chem. Phys., vol. 49, no. 8, Oct. 15, 1968, pp. 3479-3496.

38. Montagu-Pollock, H. M.; Rhodin, T. N.; and Southon, M. J.: Some Properties of Thin Metal Films Observed by Field-Ion and Field Emission Microscopy. Surface Sci, vol. 12, 1968, pp. 1-18.

39. Nishikawa, O.; and Müller, E. W.: Lattice Deformation by Mechanical and Electrical Contacts. Application of Field Ion Microscopy in Physical Metallurgy and Corrosion, Georgia Inst. Tech., Atlanta, Ga., Dec. 1969, pp. 155-176.

40. Graham, W. R.; Hutchinson, F.; Nadakavukaren, J. J.; Reed, D. A.; and Schwenterly, S. W.: Epitaxial Deposition of Platinum on Iridium at Low Temperatures. J. Appl. Phys., vol. 40, no. 10, Sept. 1969, pp. 3931-3936.

41. Avner, Sidney H.: Introduction to Physical Metallurgy. McGraw-Hill Book Co., Inc., 1964.

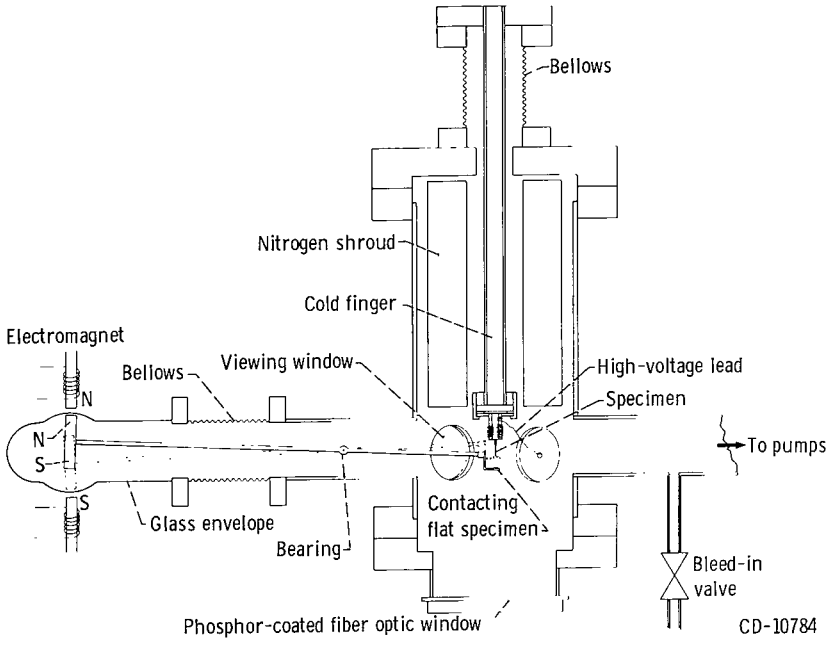

Figure 1. - Field ion/emission microscope adhesion apparatus.

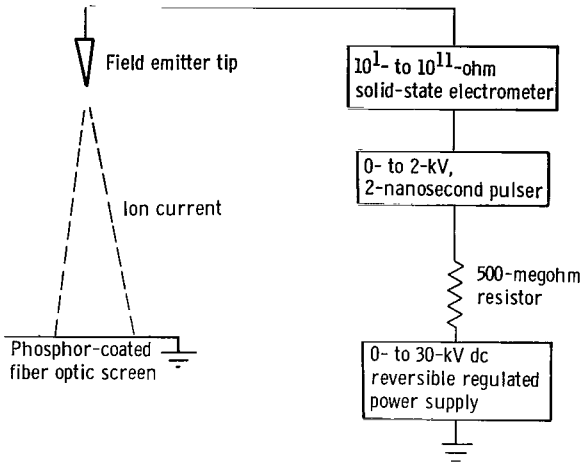

Figure 2. - Electrical schematic for field ion microscope.

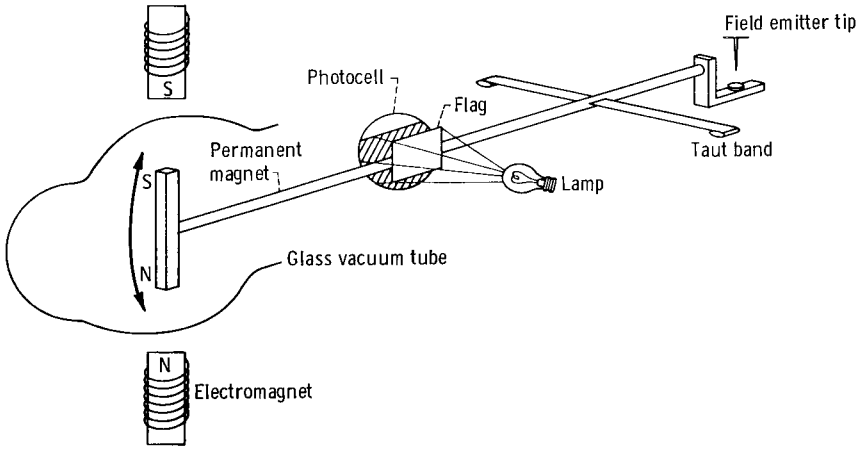

Figure 3. - Field-ion-microscope emitter tip contact apparatus.

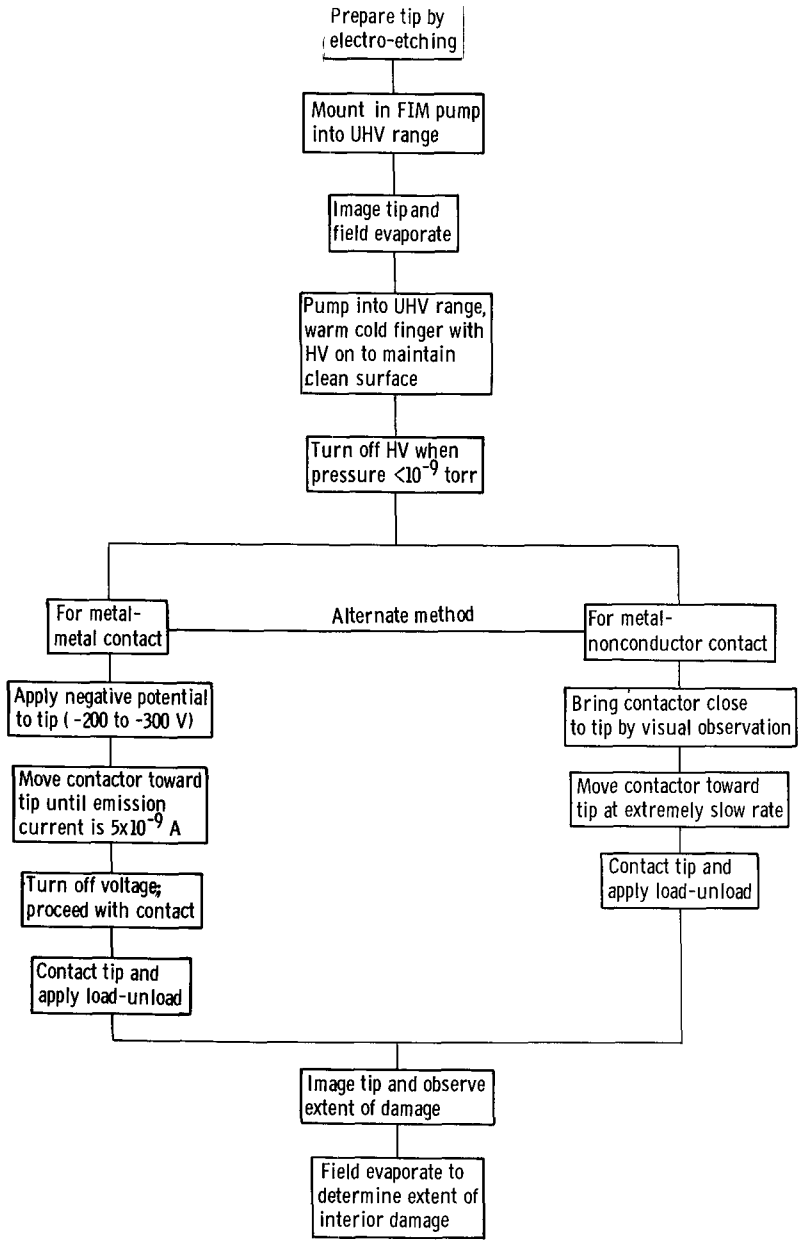

Figure 4. - Flow diagram of field-ion-microscope (FIM) tip contact procedure.

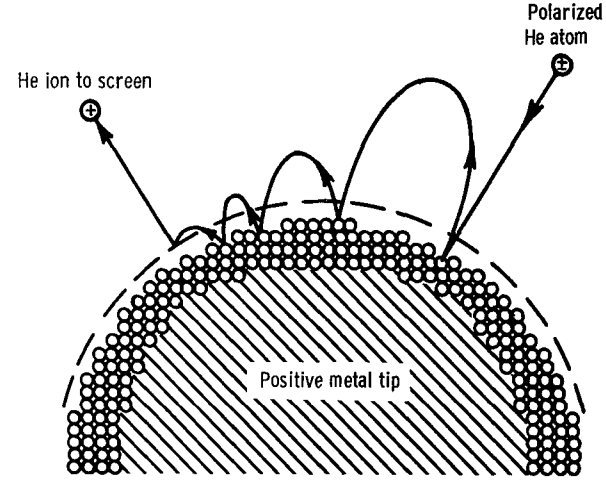

Figure 5. - Field ionization-image formation. (From ref. 14.)

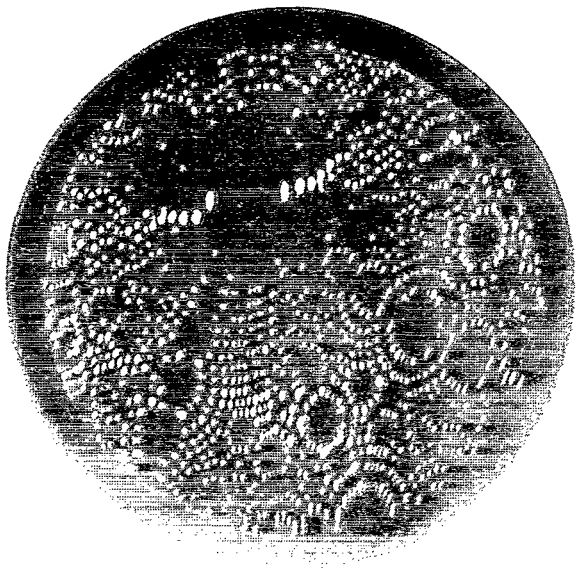

(a) Before exposure.

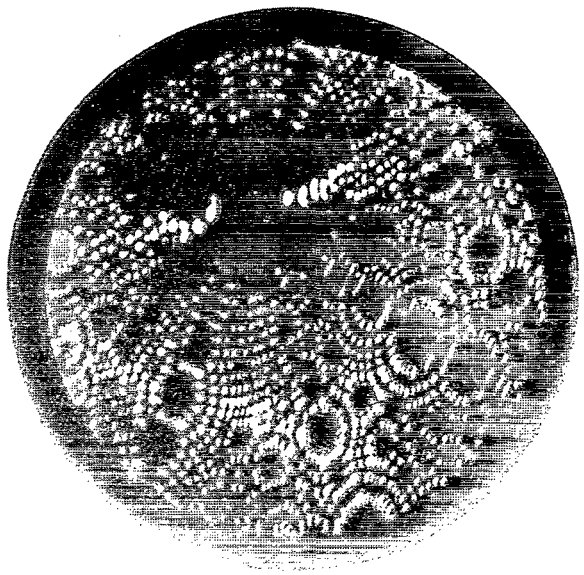

(b) After exposure of 6×10^{-10} torr at 300 K for 60 minutes.

Figure 6. - Field ion micrographs of tungsten tip. Voltage, 9.9 kilovolts; liquid-helium cooling; helium image gas.

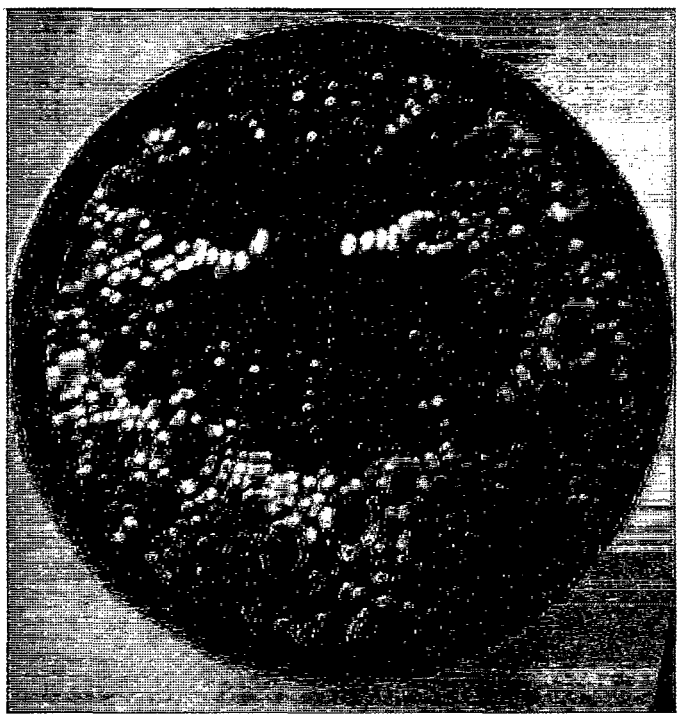

Figure 7. - Color superposition of micrographs in figures 6(a) and (b).

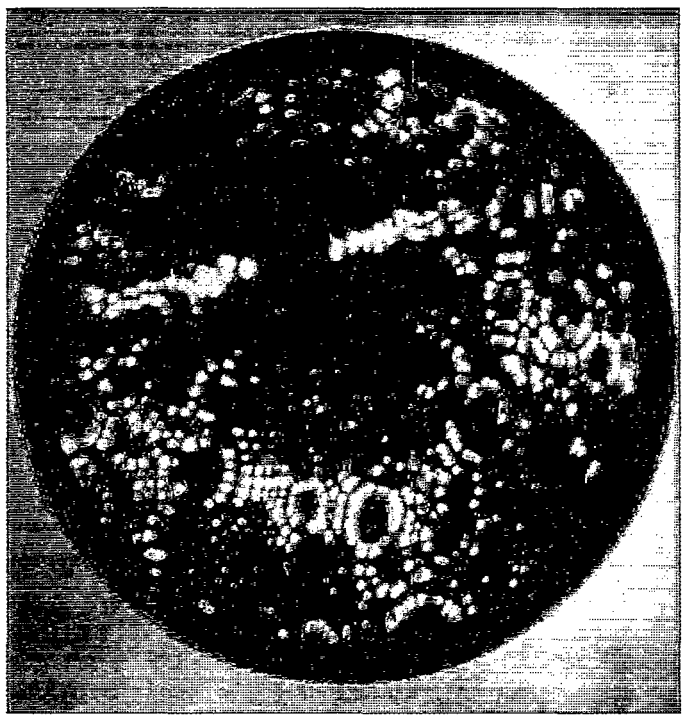

Figure 8. - Color superposition of tungsten tip before and after exposure at 2×10^{-9} torr for 35 minutes at 78 K.

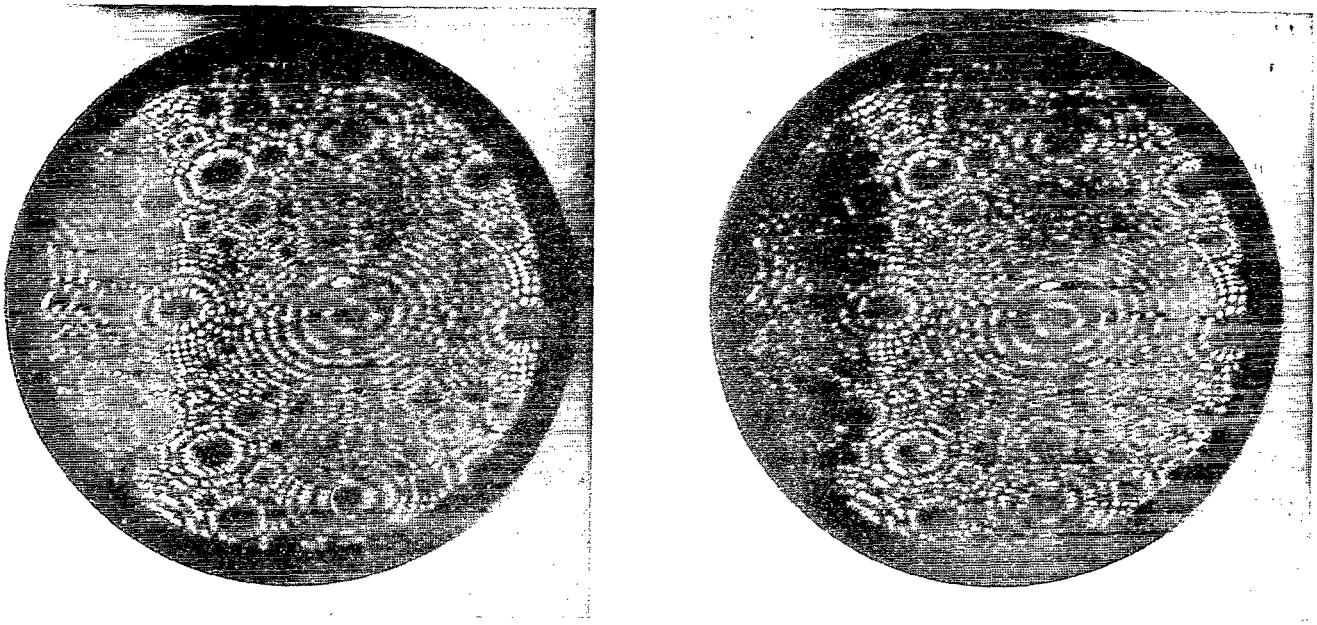

(a) Before exposure.

(b) After exposure of 2×10^{-10} torr at 78 K for 60 minutes.

Figure 9. - Field ion micrographs of iridium tip. Voltage, 10.0 kilovolts; liquid-helium cooling; helium image gas.

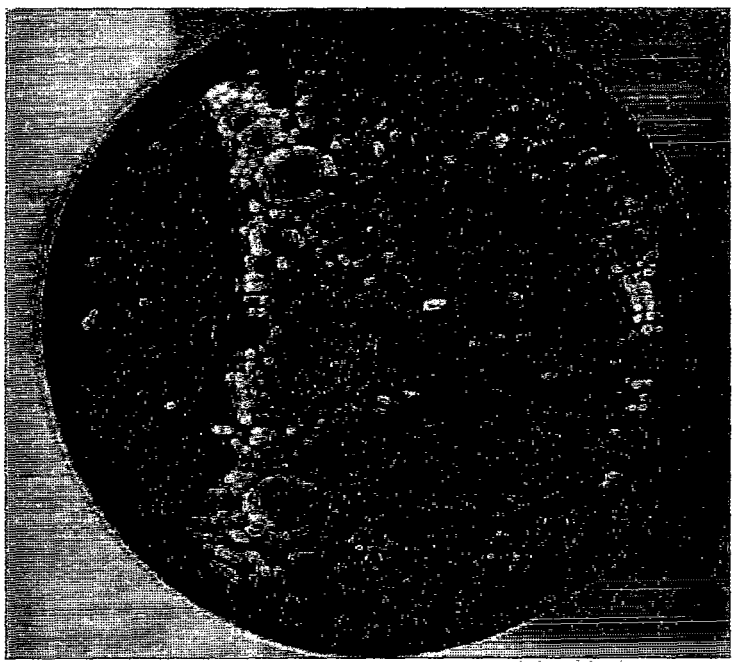

Figure 10. - Color superposition of micrographs in figures 9(a) and (b).

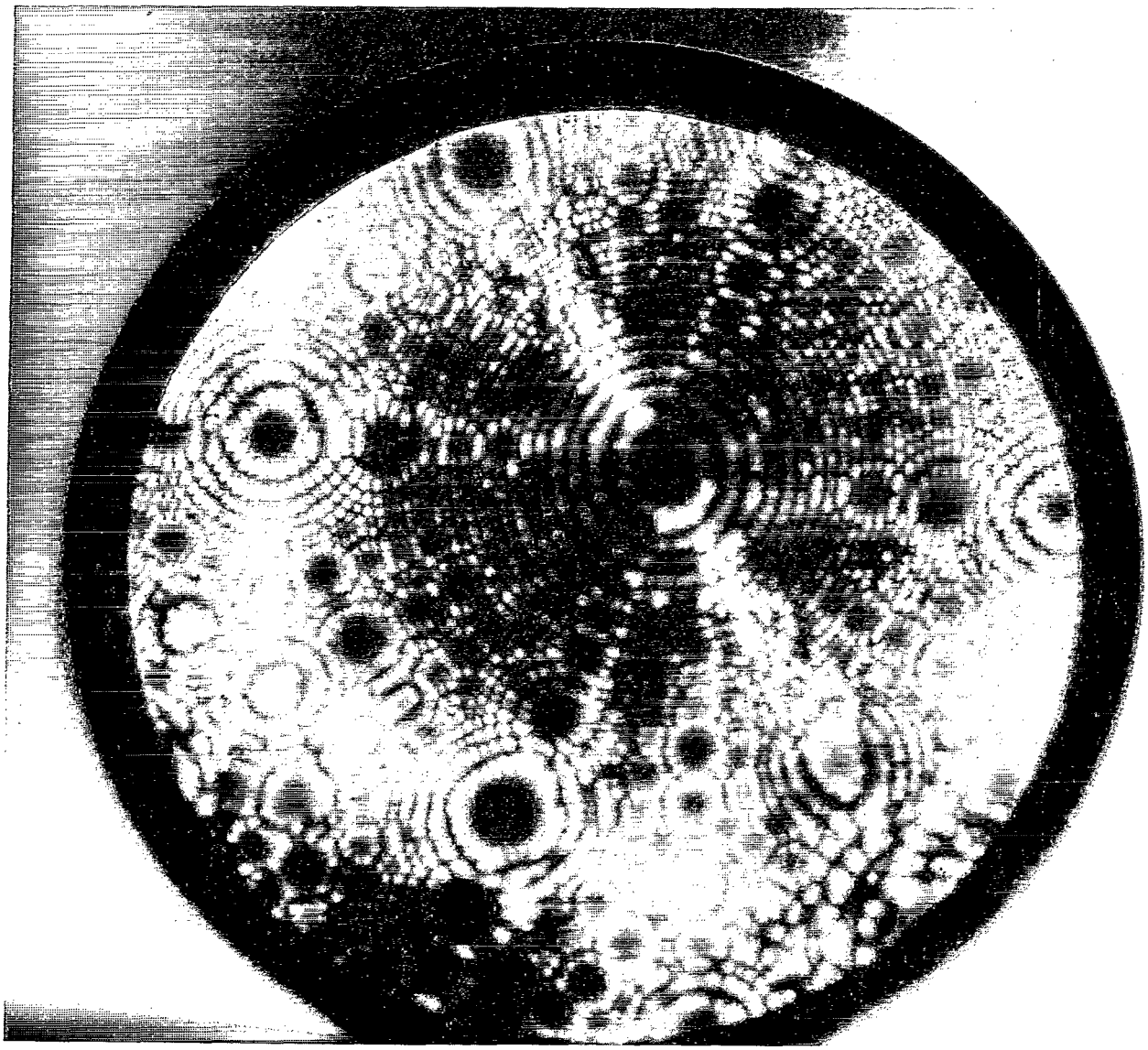

(a) Tungsten prior to contact. Voltage, 16.0 kilovolts.

Figure 11. - Field ion micrographs of tungsten-platinum contact. Image gas, helium.

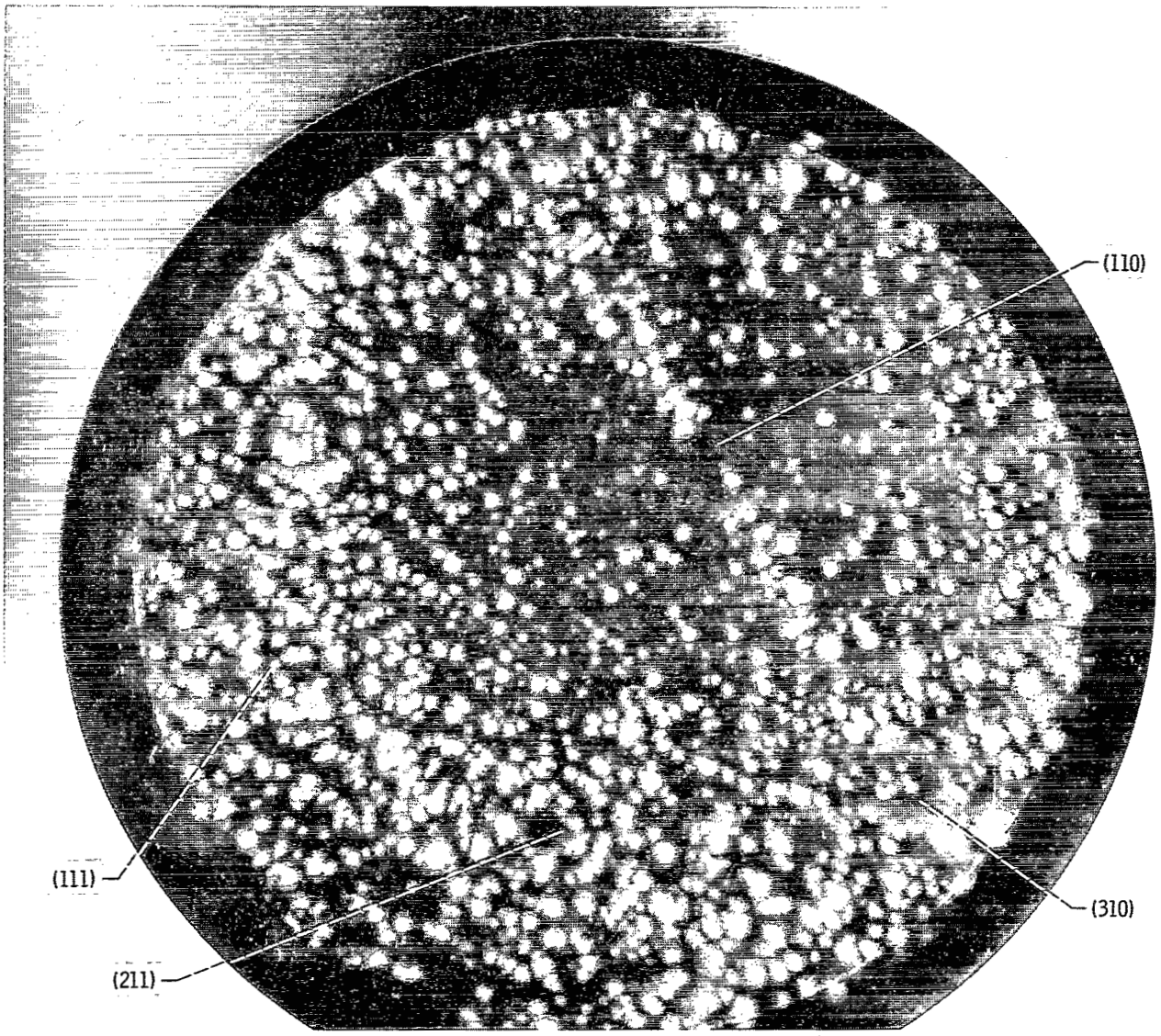

(b) Tungsten after platinum contact at 14.0 kilovolts.

Figure 11. - Continued.

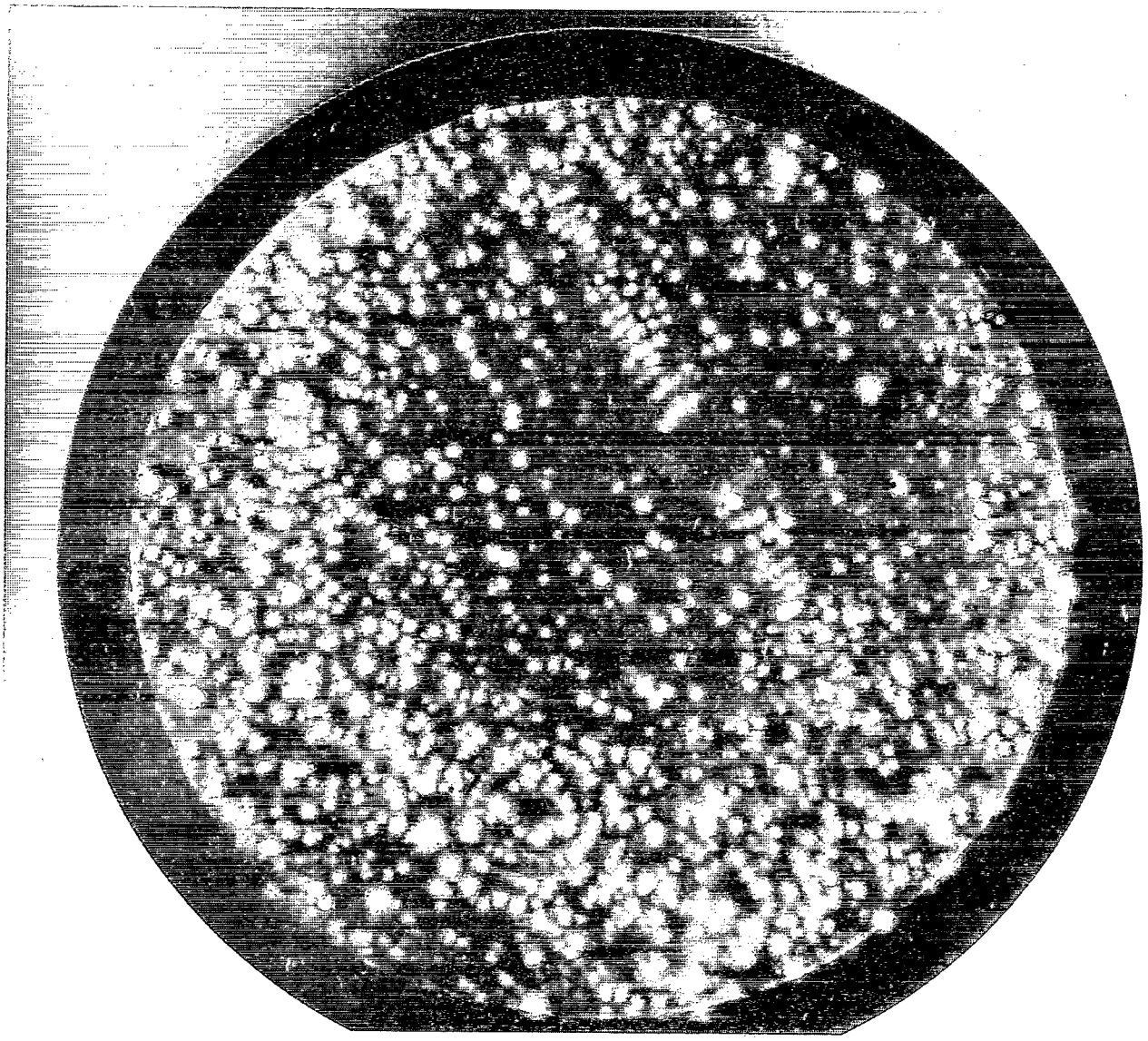

(c) Tungsten after platinum contact at 14.5 kilovolts.

Figure 11. - Continued.

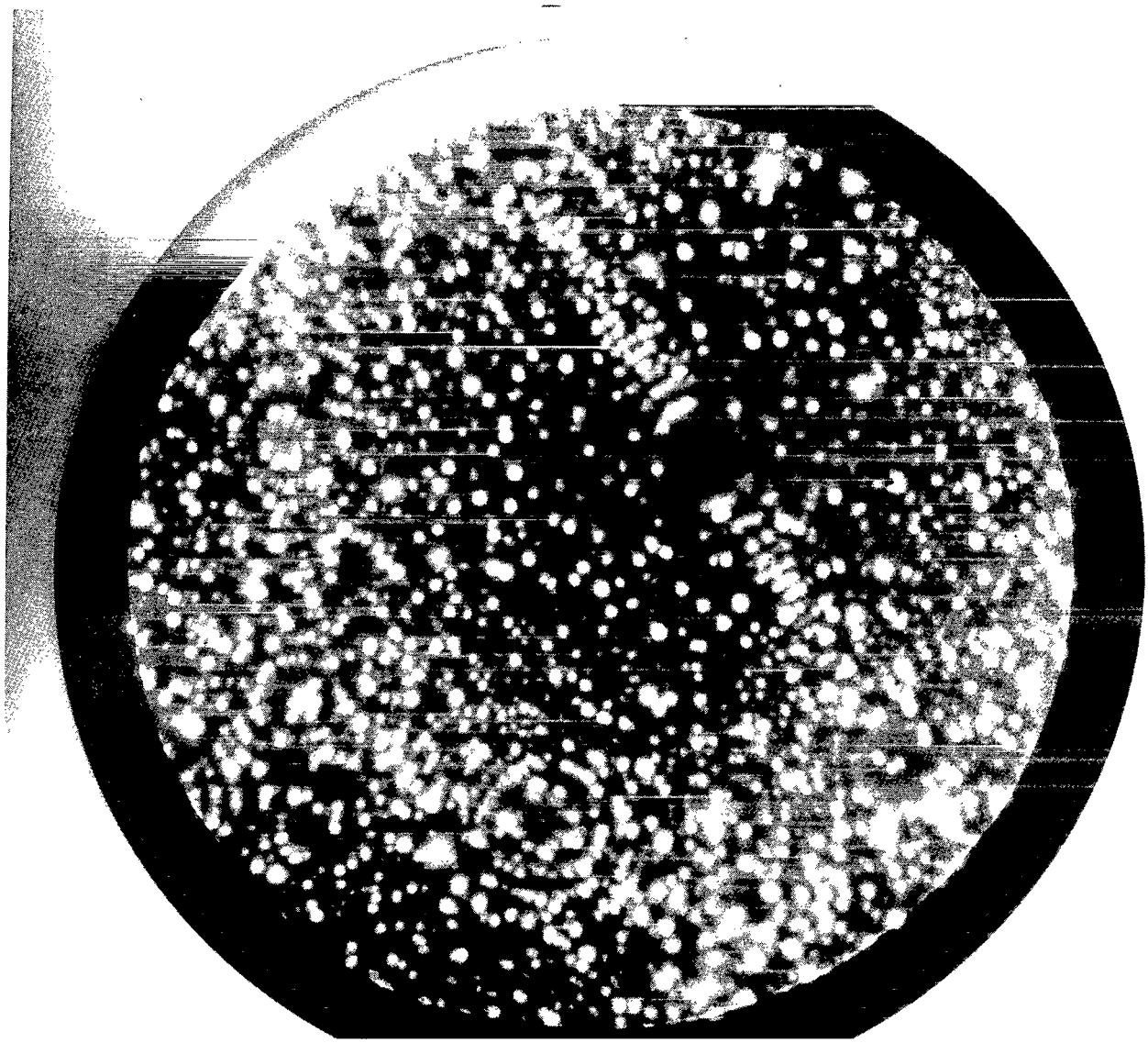

(d) Tungsten after platinum contact at 15.0 kilovolts.

Figure 11. - Continued.

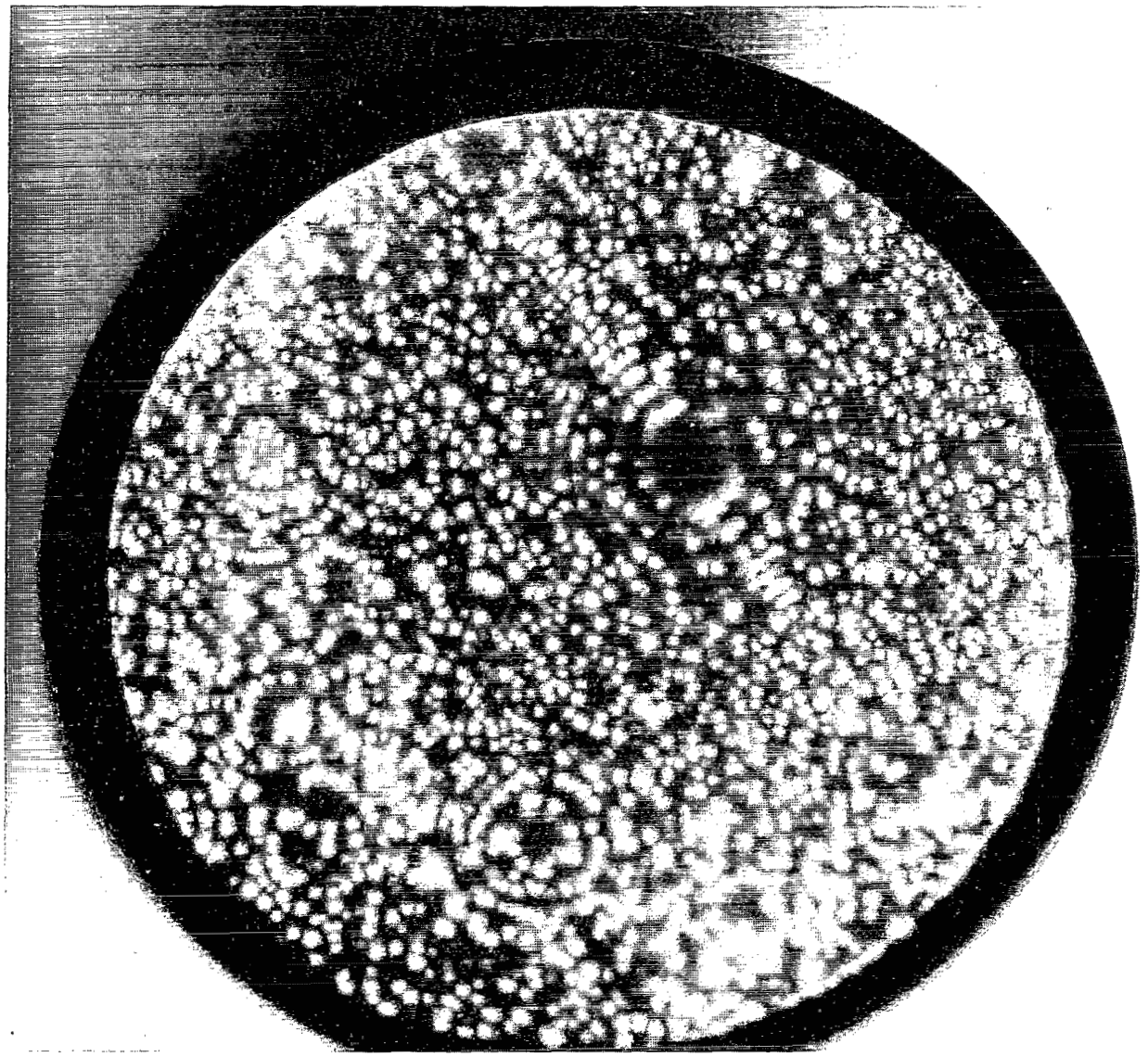

(e) Tungsten after platinum contact at 15.5 kilovolts.

Figure 11. - Continued.

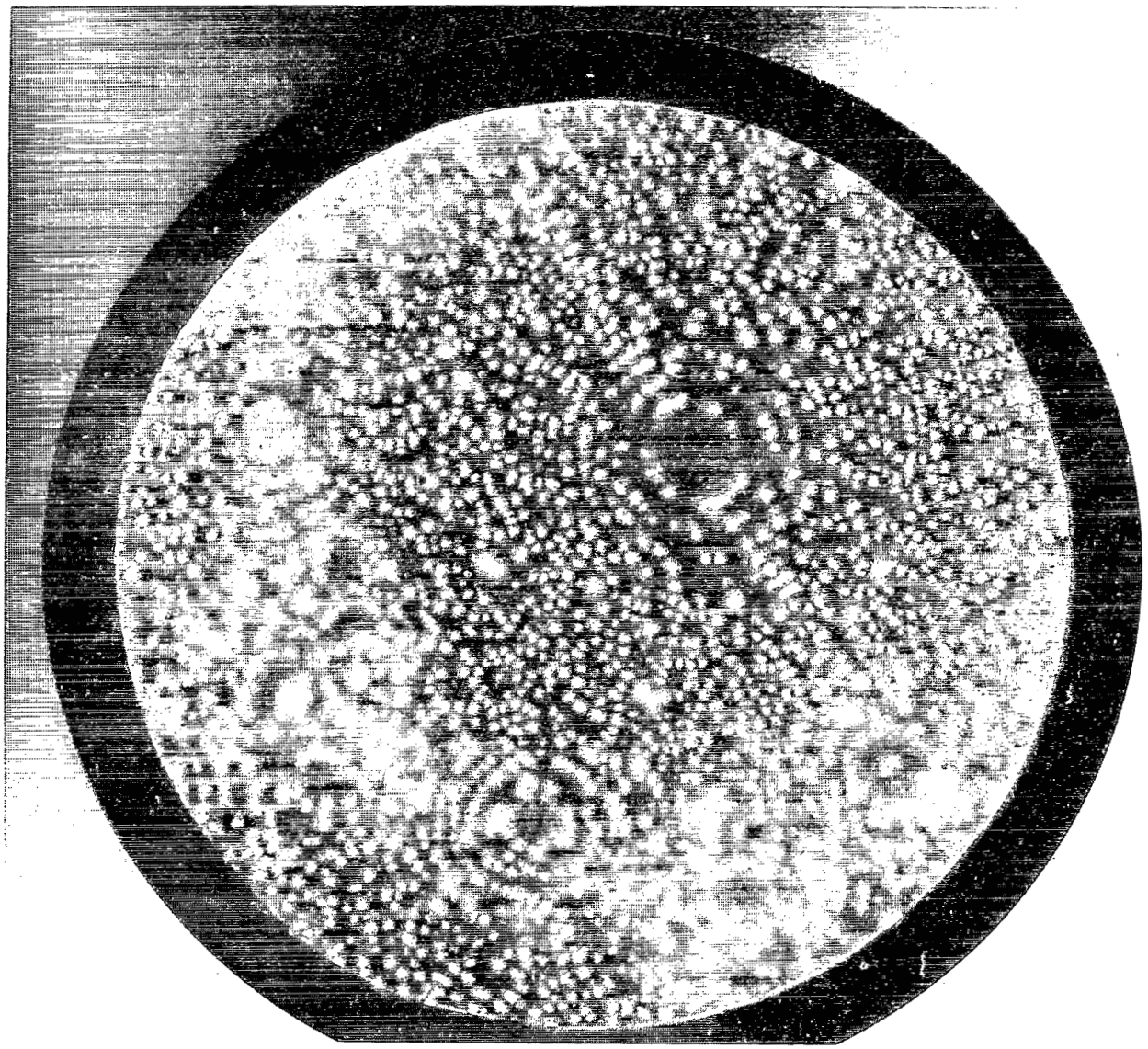

(f) Tungsten after platinum contact at 16.0 kilovolts.

Figure 11. - Continued.

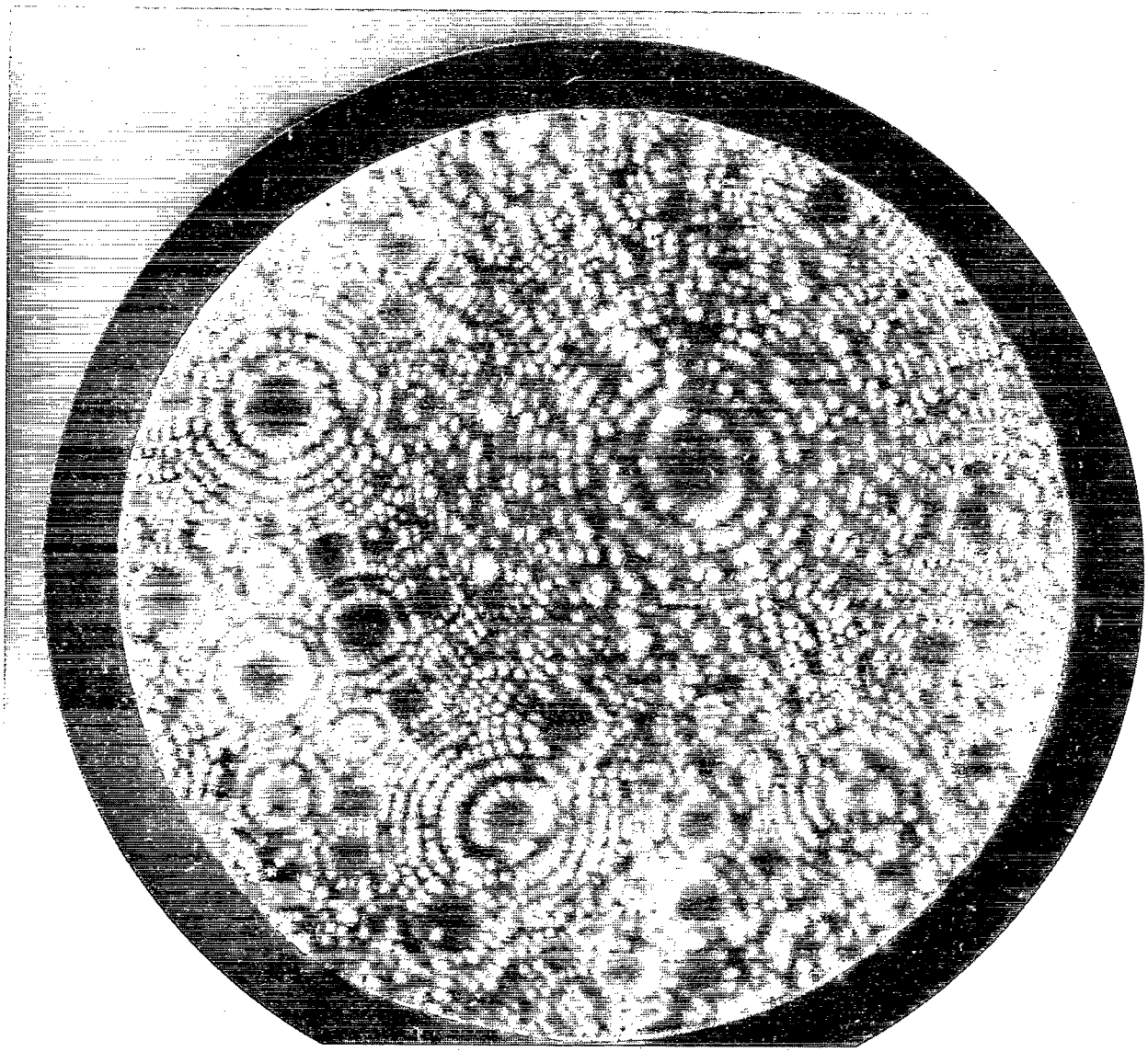

(g) Tungsten after platinum contact at 16.0 kilovolts and some field evaporation; liquid-nitrogen cooling.

Figure 11. - Continued.

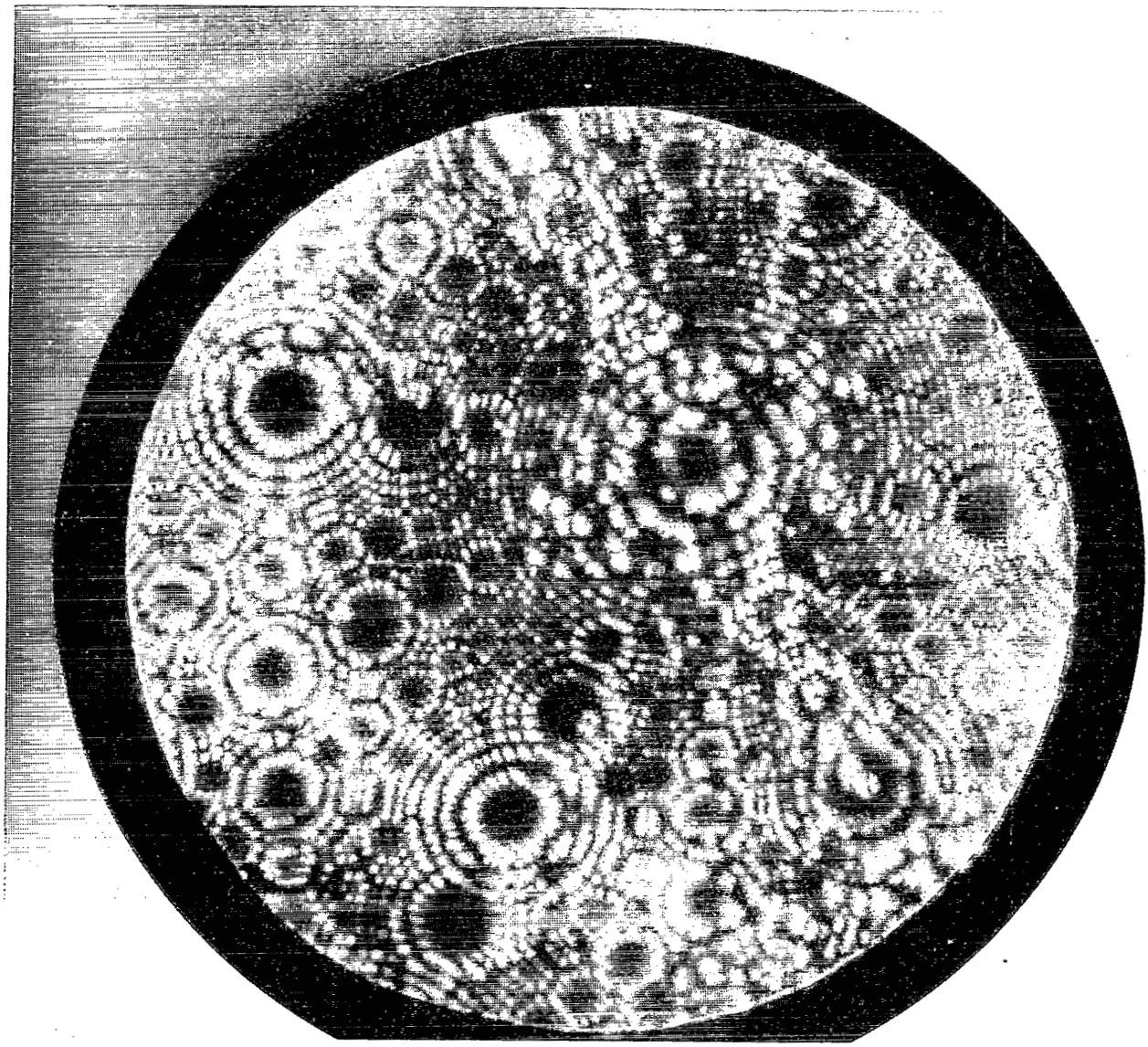

(h) Tungsten after platinum contact at 16.0 kilovolts and further field evaporation; liquid-nitrogen cooling.

Figure 11. - Continued.

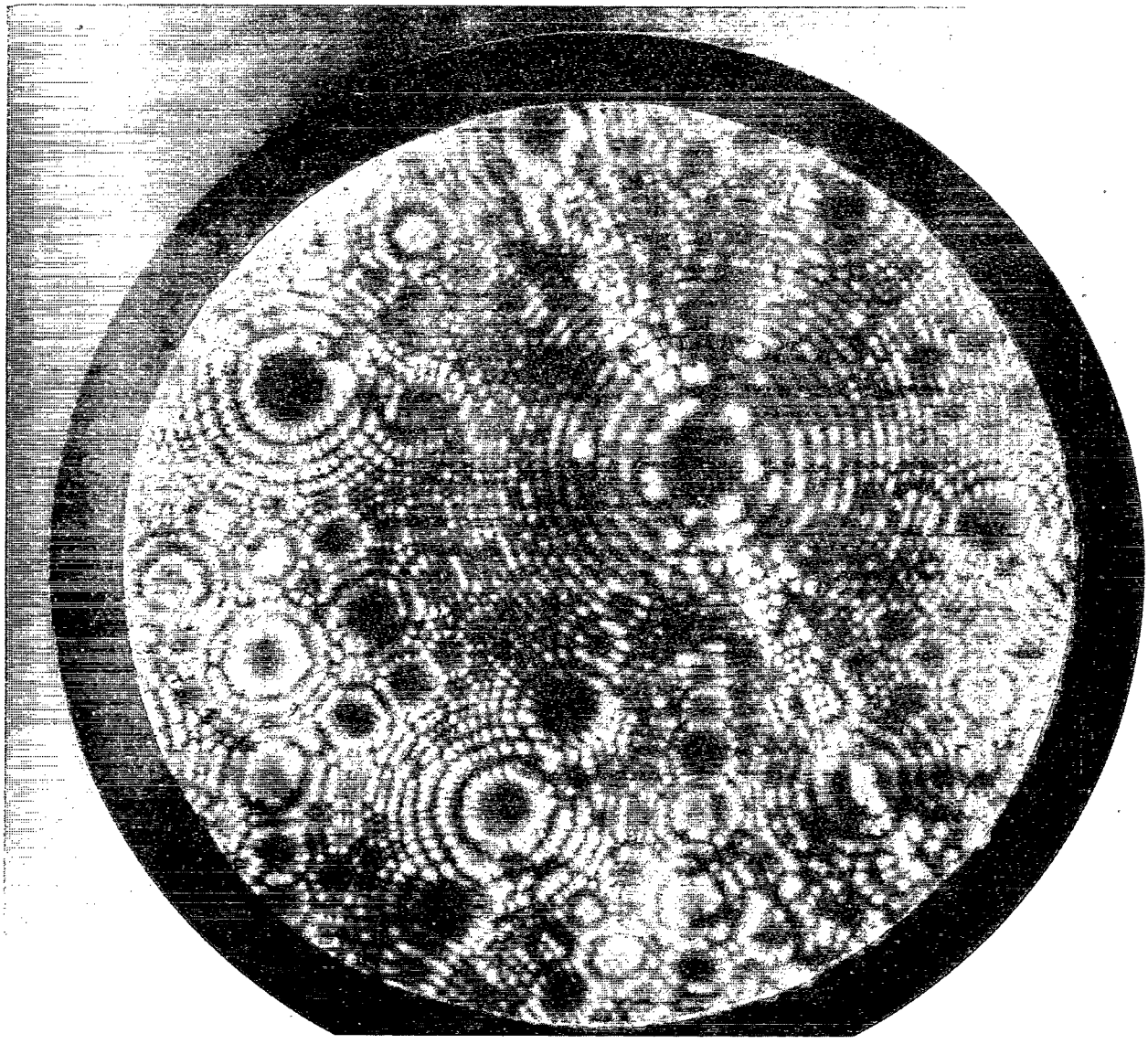

(i) Tungsten completely cleaned after platinum contact at 16.0 kilovolts.

Figure 11. - Concluded.

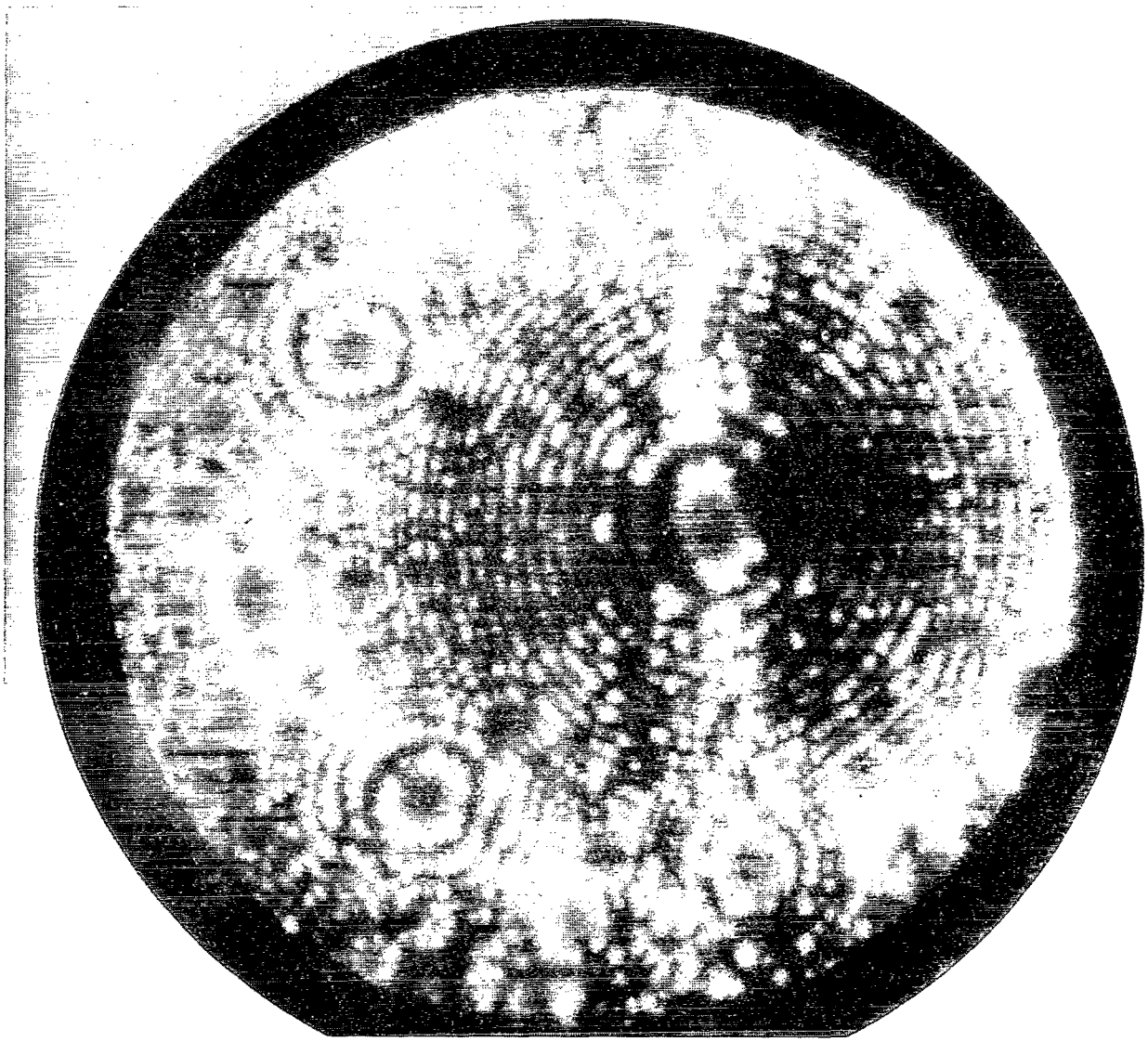

(a) Tungsten prior to contact. Voltage, 13.0 kilovolts; liquid-nitrogen cooling.

Figure 12. - Field ion micrographs of tungsten-gold contact. Image gas, helium.

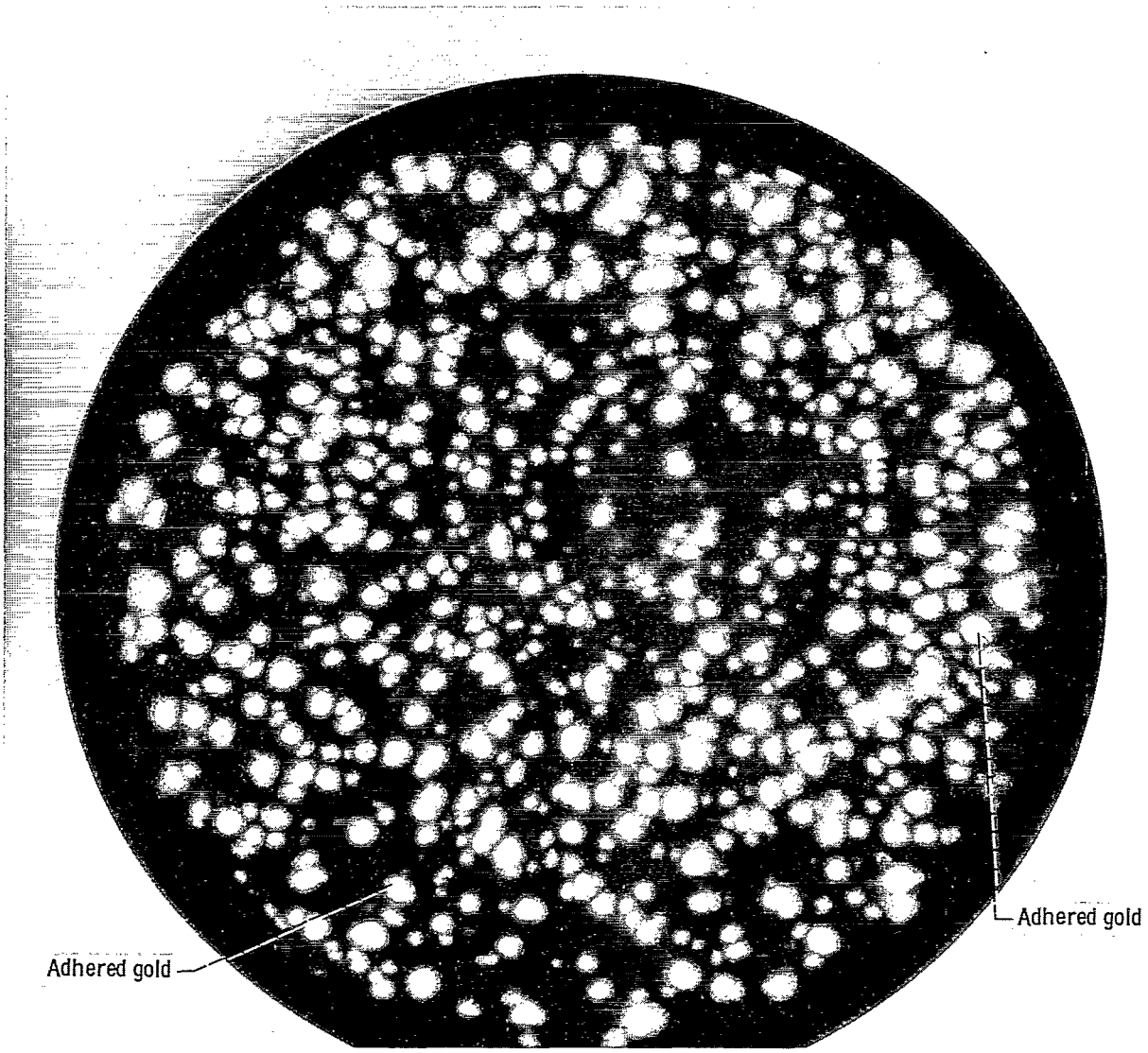

(b) Tungsten after gold contact at 11.0 kilovolts; liquid-nitrogen cooling.

Figure 12. - Continued.

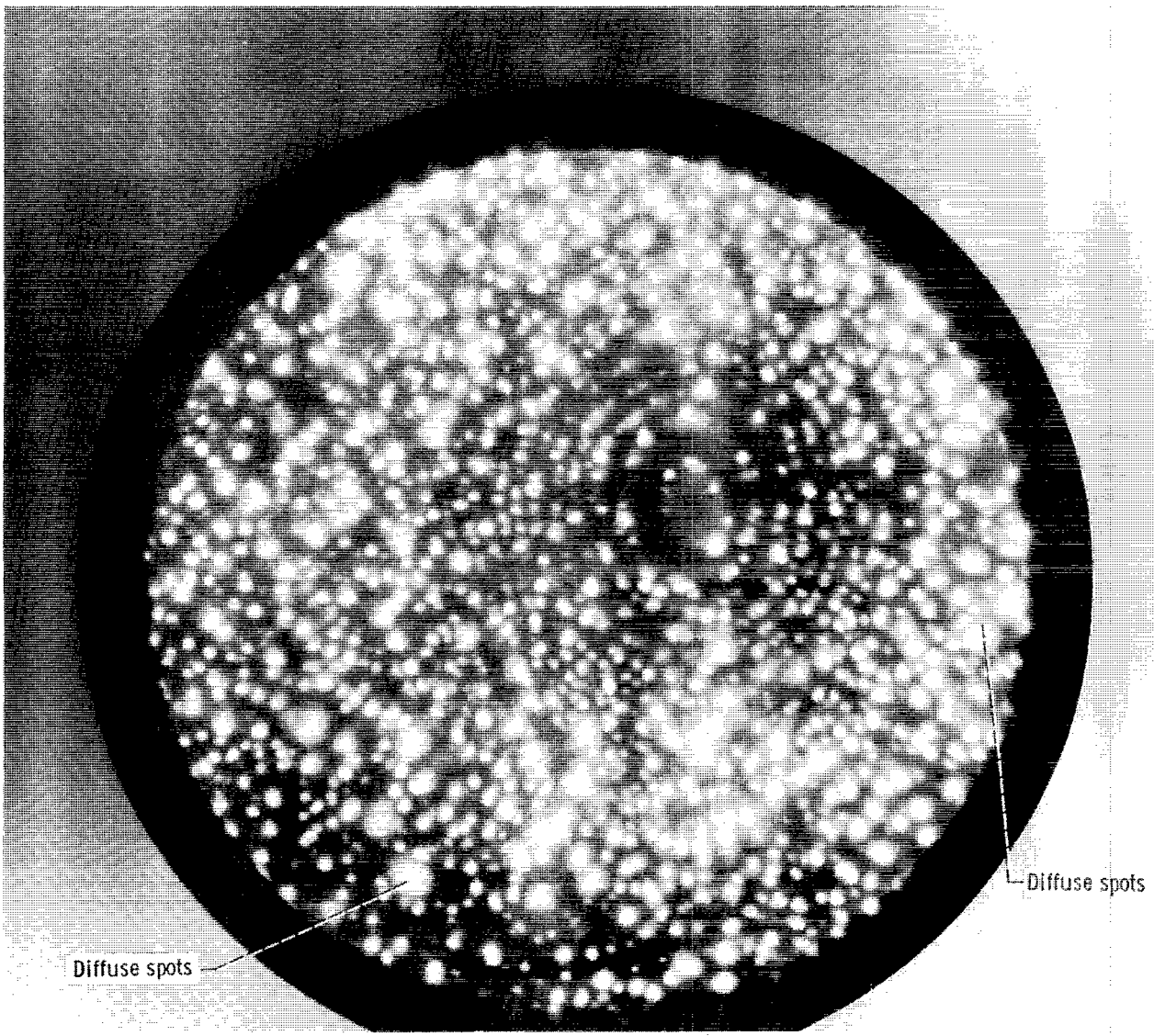

(c) Tungsten after gold contact at 13.0 kilovolts; liquid-helium cooling.

Figure 12. - Continued.

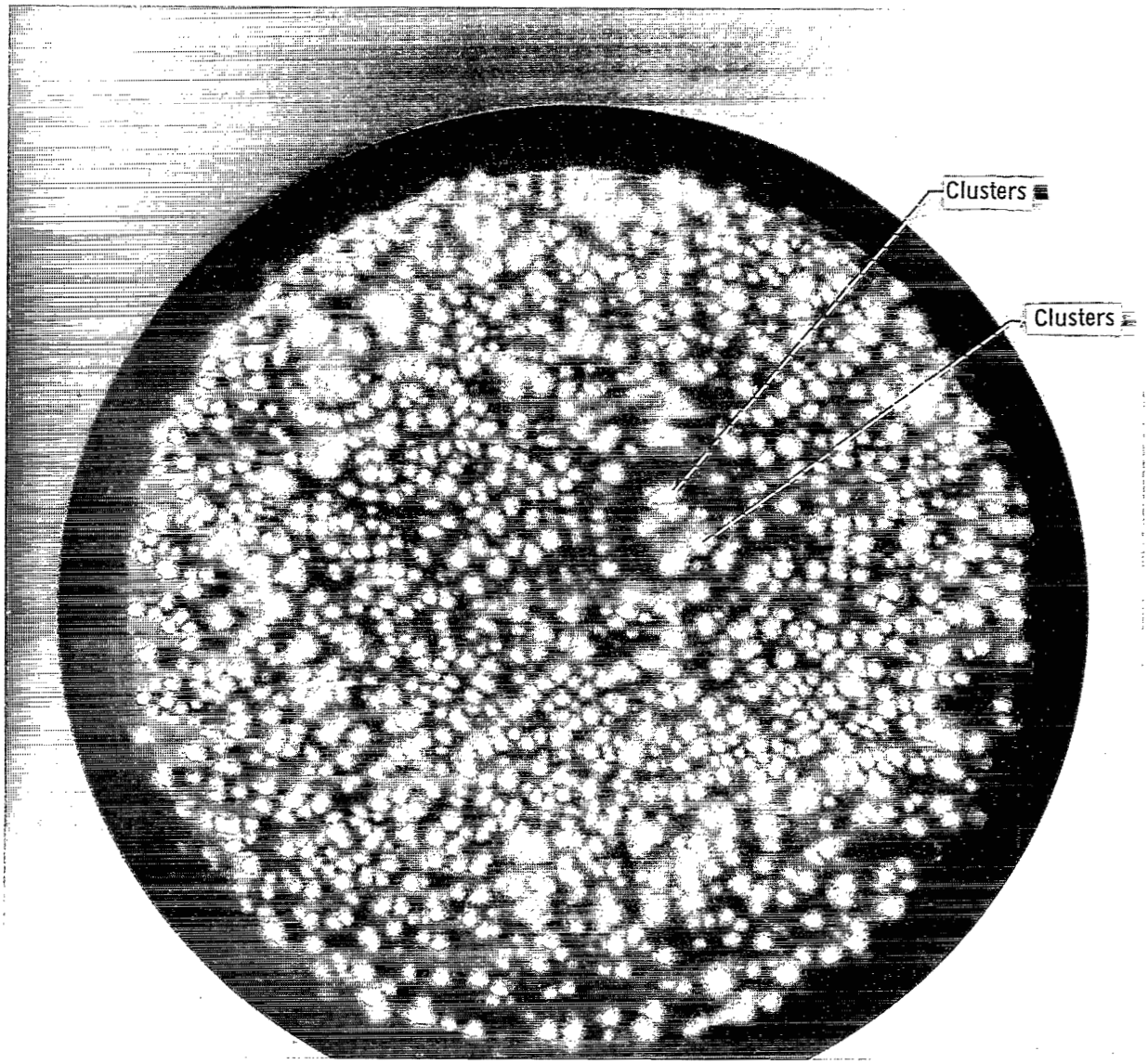

(d) Tungsten after gold contact at 13.0 kilovolts with voltage raised to 14.5 kilovolts for 30 seconds; liquid-helium cooling.

Figure 12. - Continued.

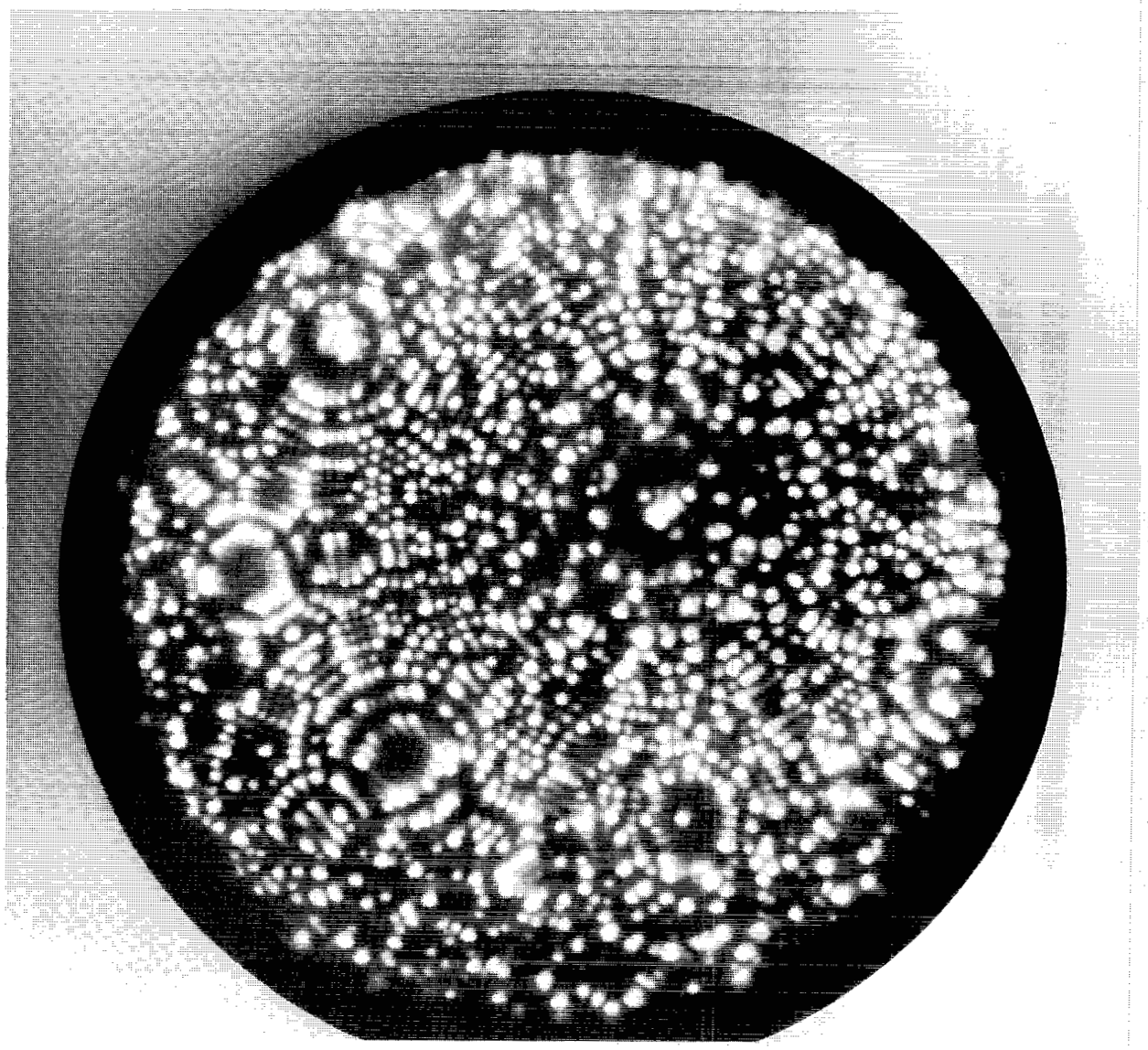

(e) Tungsten after gold contact at 13.0 kilovolts with voltage raised to 15.5 kilovolts for 30 seconds; liquid-helium cooling.

Figure 12. - Continued.

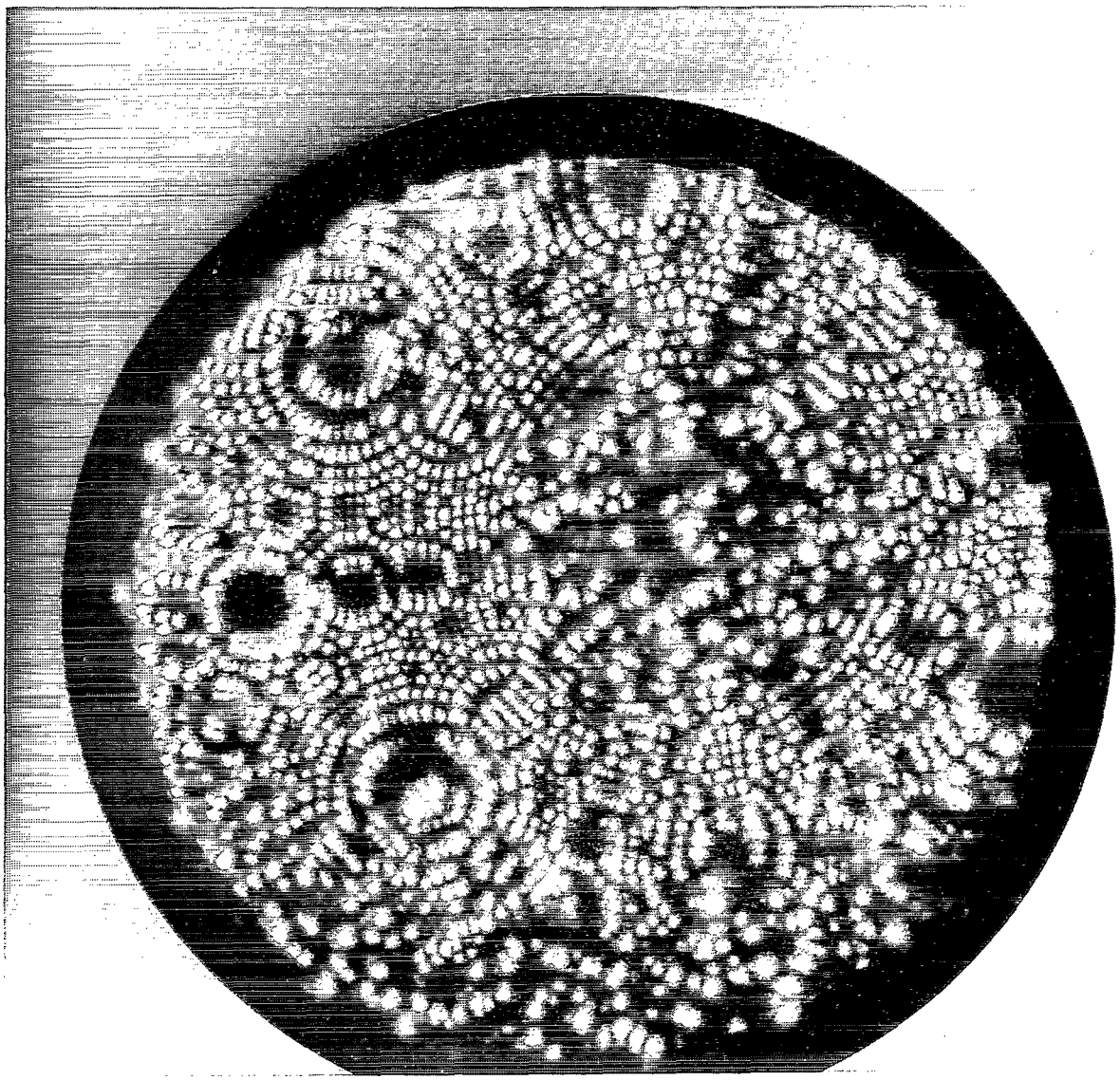

(f) Tungsten after gold contact at 13.0 kilovolts with voltage raised to 16.0 kilovolts for 10 seconds; liquid-helium cooling.

Figure 12. - Concluded.

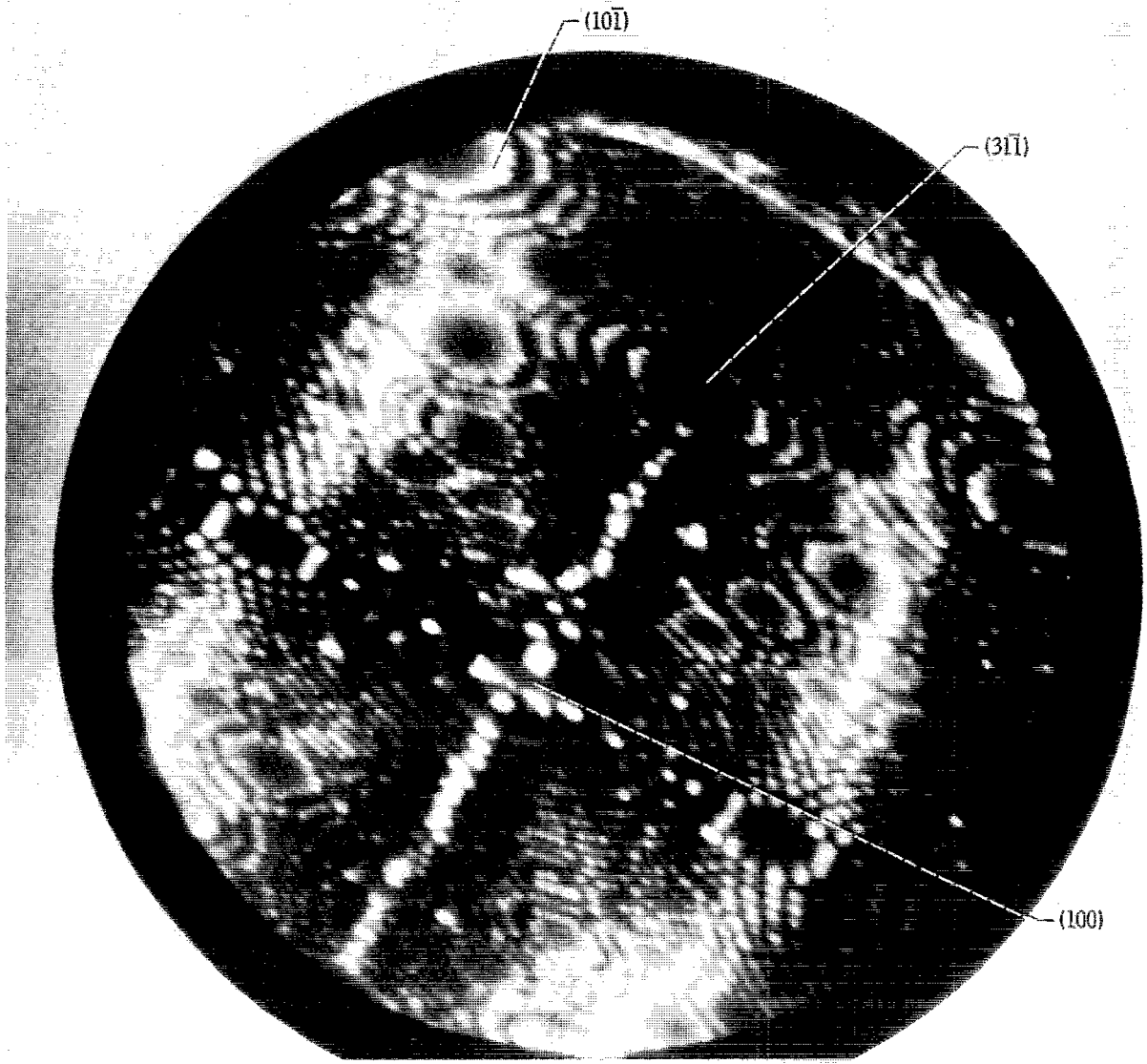

(a) Iridium prior to contact. Voltage, 13.0 kilovolts; liquid-nitrogen cooling.

Figure 13. - Field ion micrographs of iridium-gold contact. Image gas, helium.

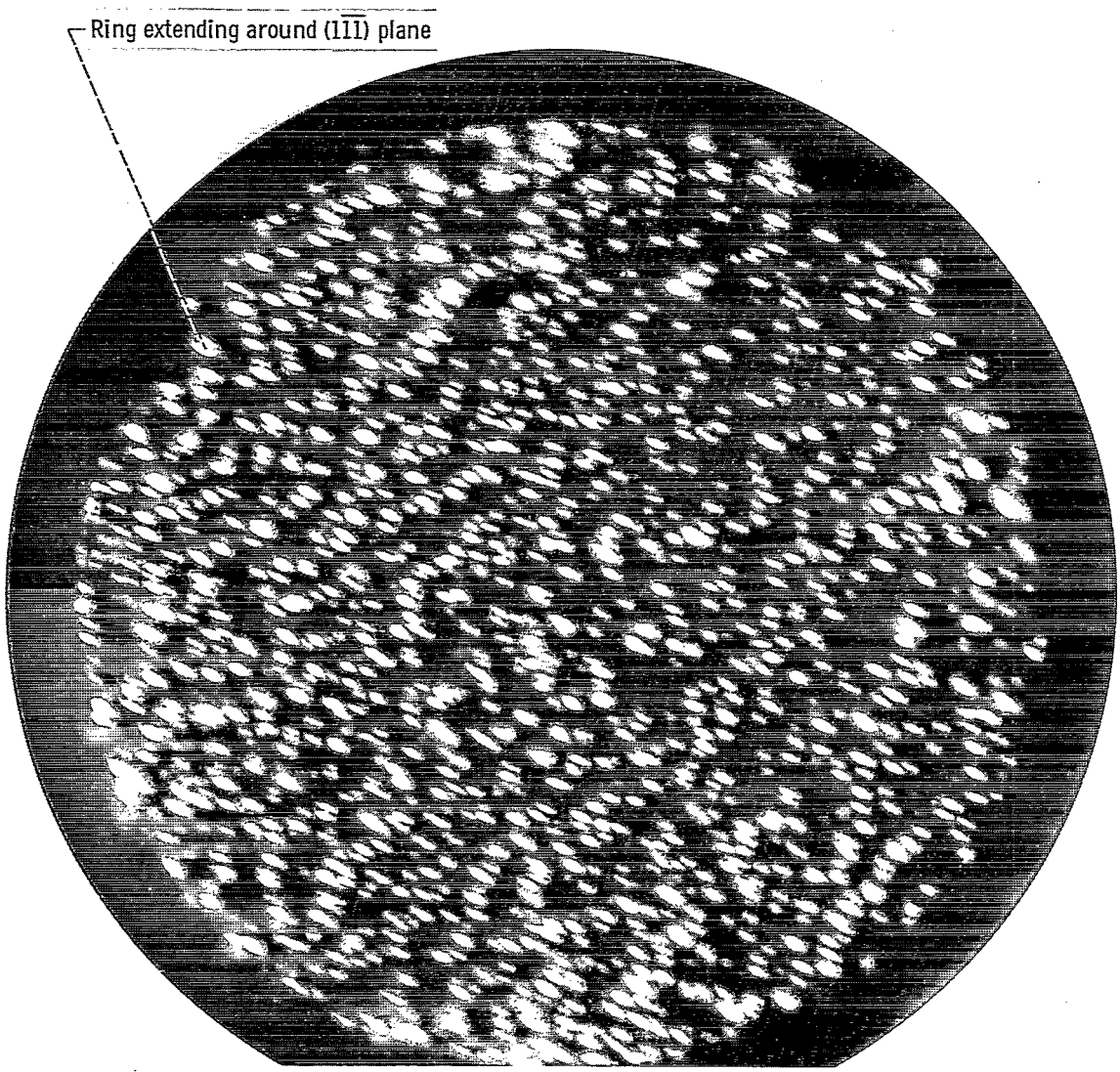

(b) Iridium after contact at 12.0 kilovolts; liquid-helium cooling.

Figure 13. - Continued.

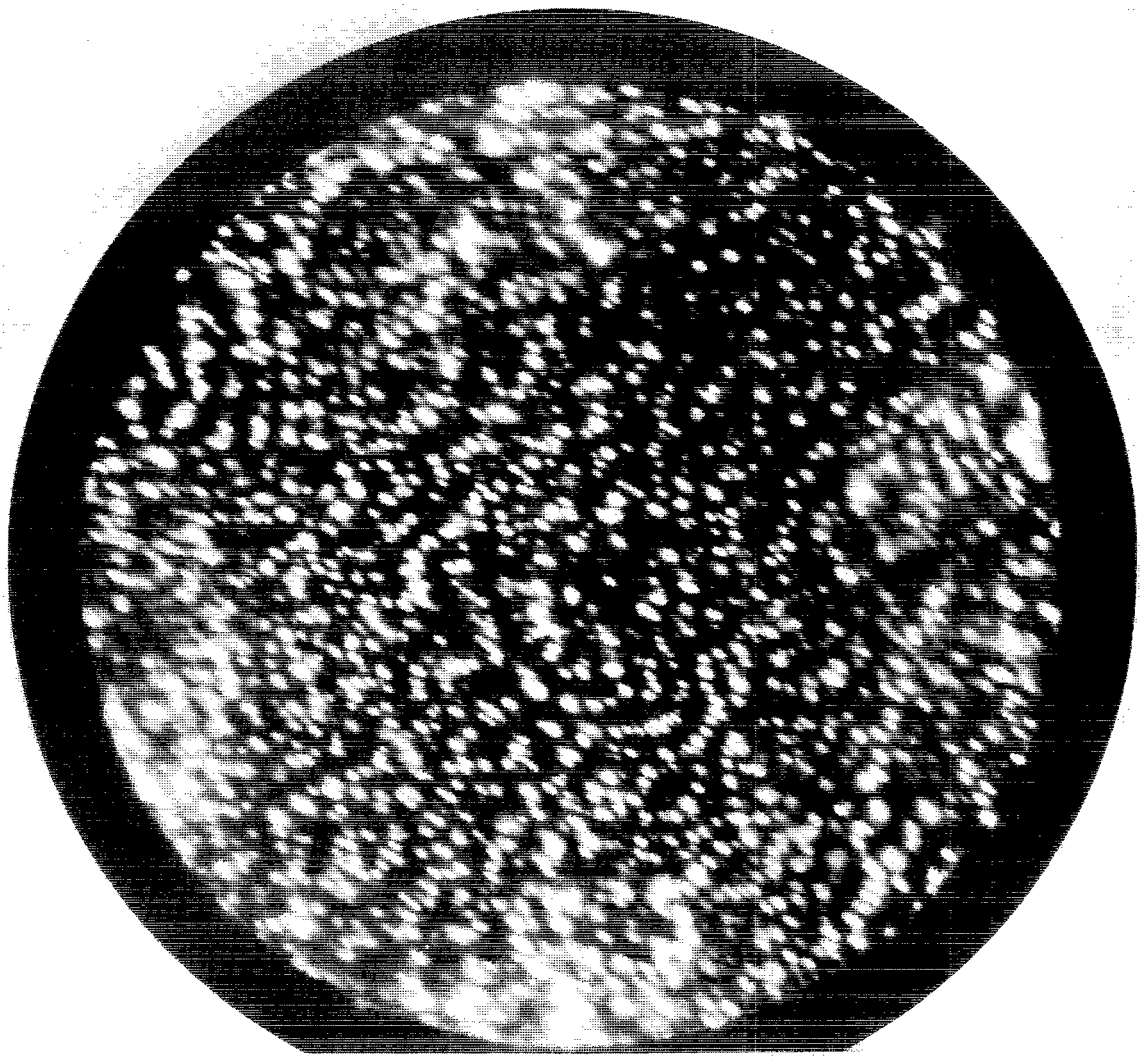

(c) Iridium after gold contact at 13.0 kilovolts; liquid-helium cooling.

Figure 13. - Continued.

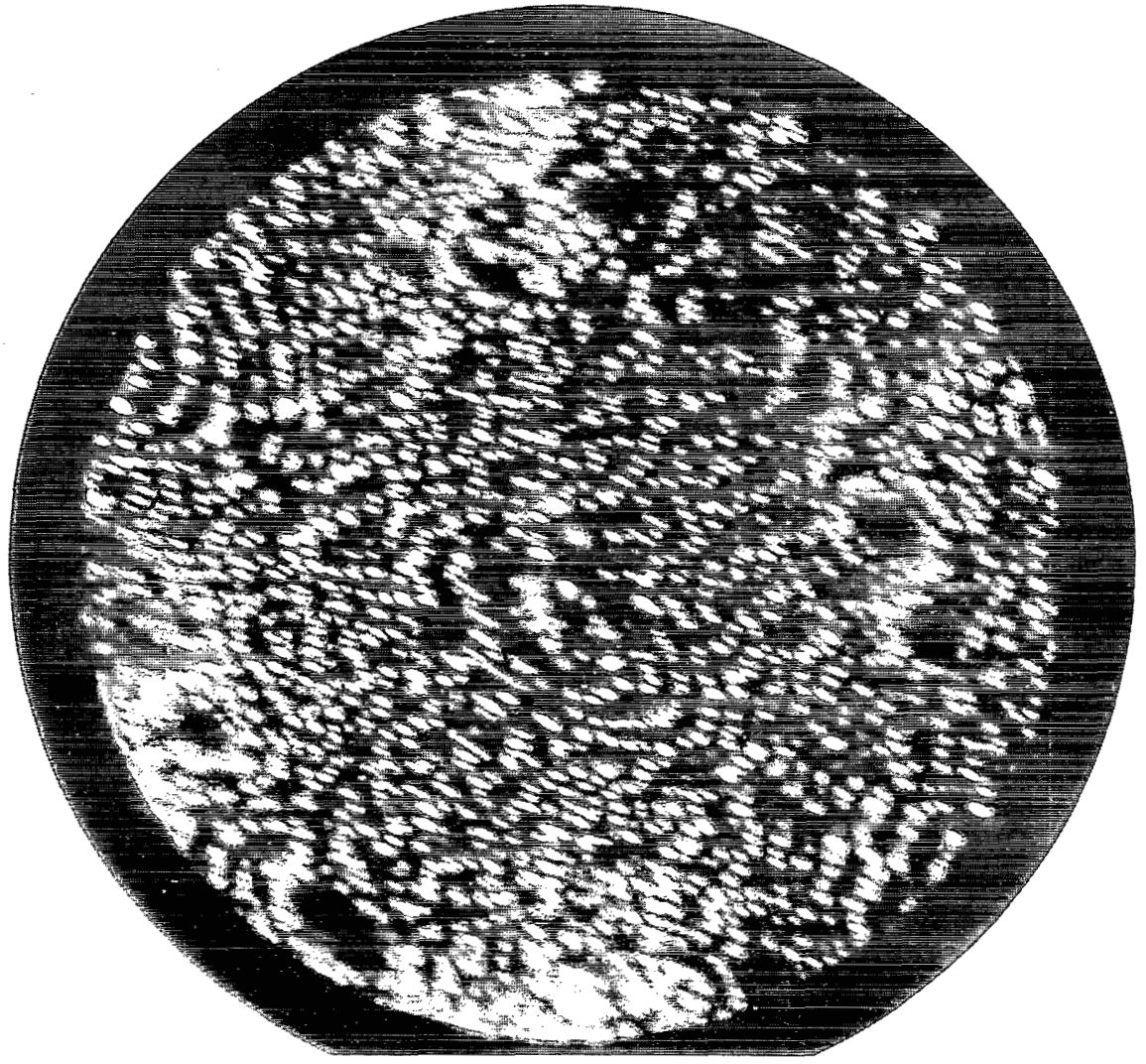

(d) Iridium after gold contact at 13.0 kilovolts with voltage raised to 14.0 kilovolts for 30 seconds; liquid-helium cooling.

Figure 13. - Continued.

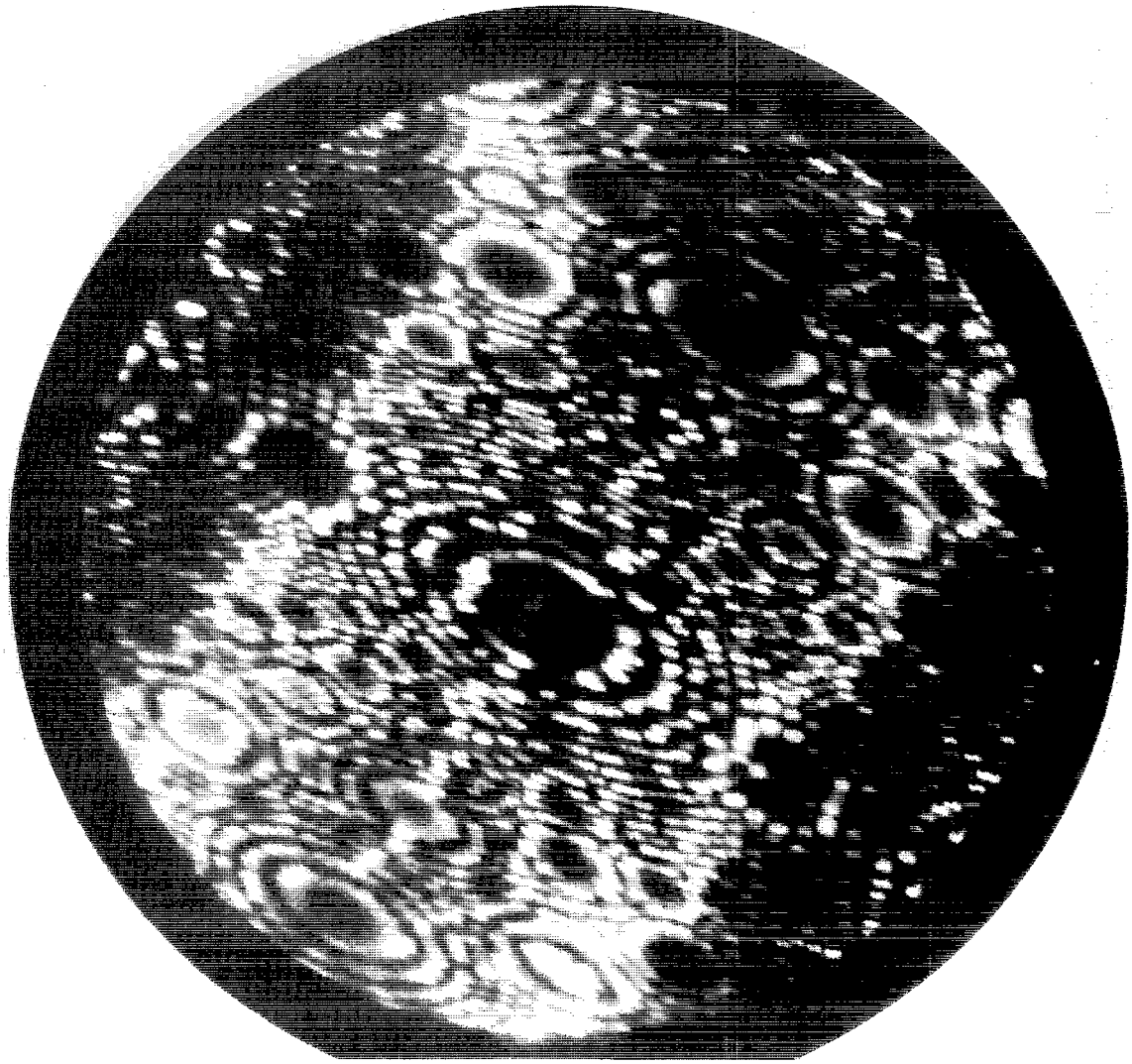

(e) Iridium after gold contact at 13.0 kilovolts with voltage raised to 15.2 kilovolts for 30 seconds; liquid-helium cooling.

Figure 13. - Concluded.

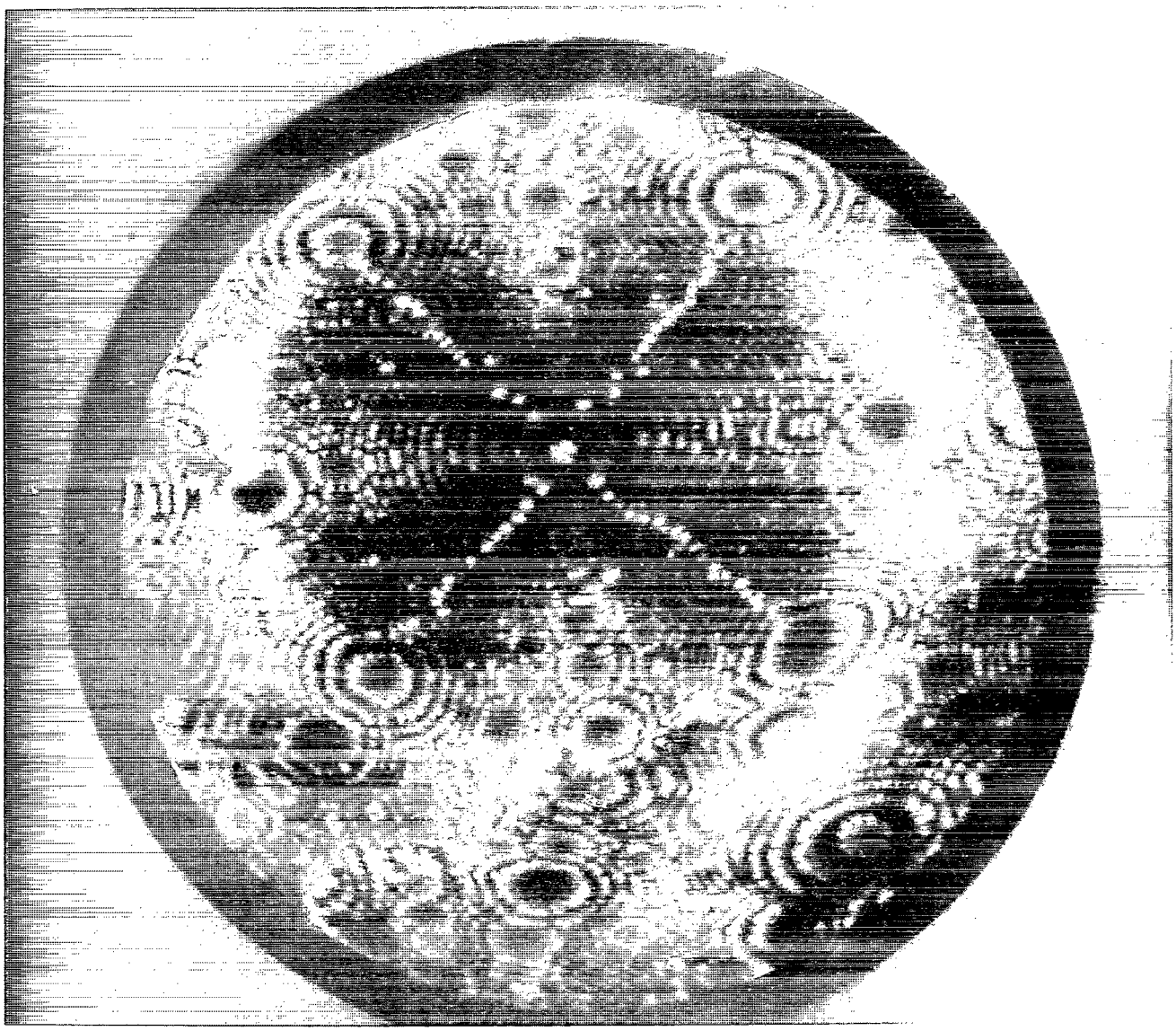

(a) Iridium prior to contact.

Figure 14. - Field ion micrographs of iridium-platinum contact. Image gas, helium; liquid-nitrogen cooling.

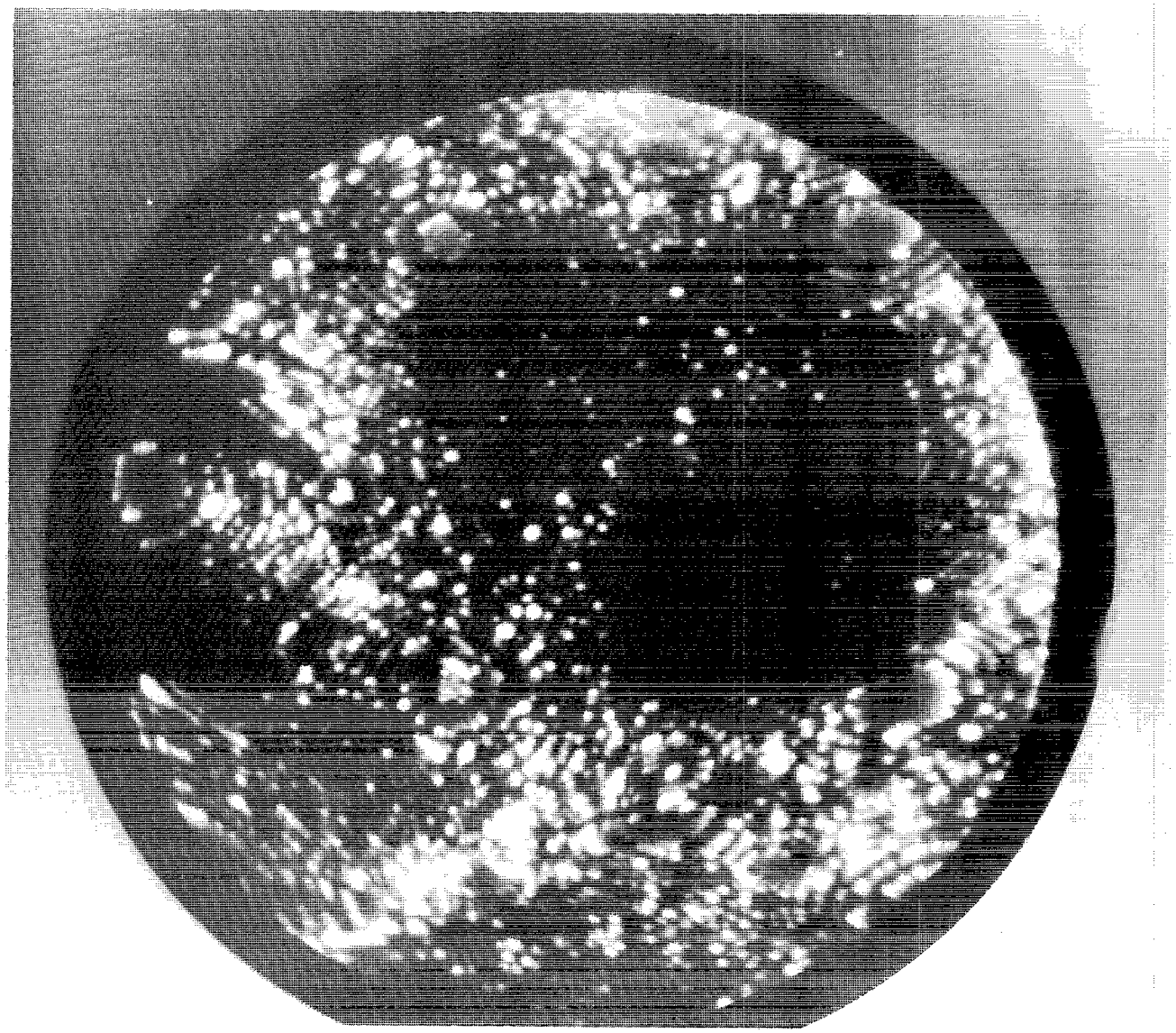

(b) Iridium after platinum contact at 18.0 kilovolts.

Figure 14. - Continued.

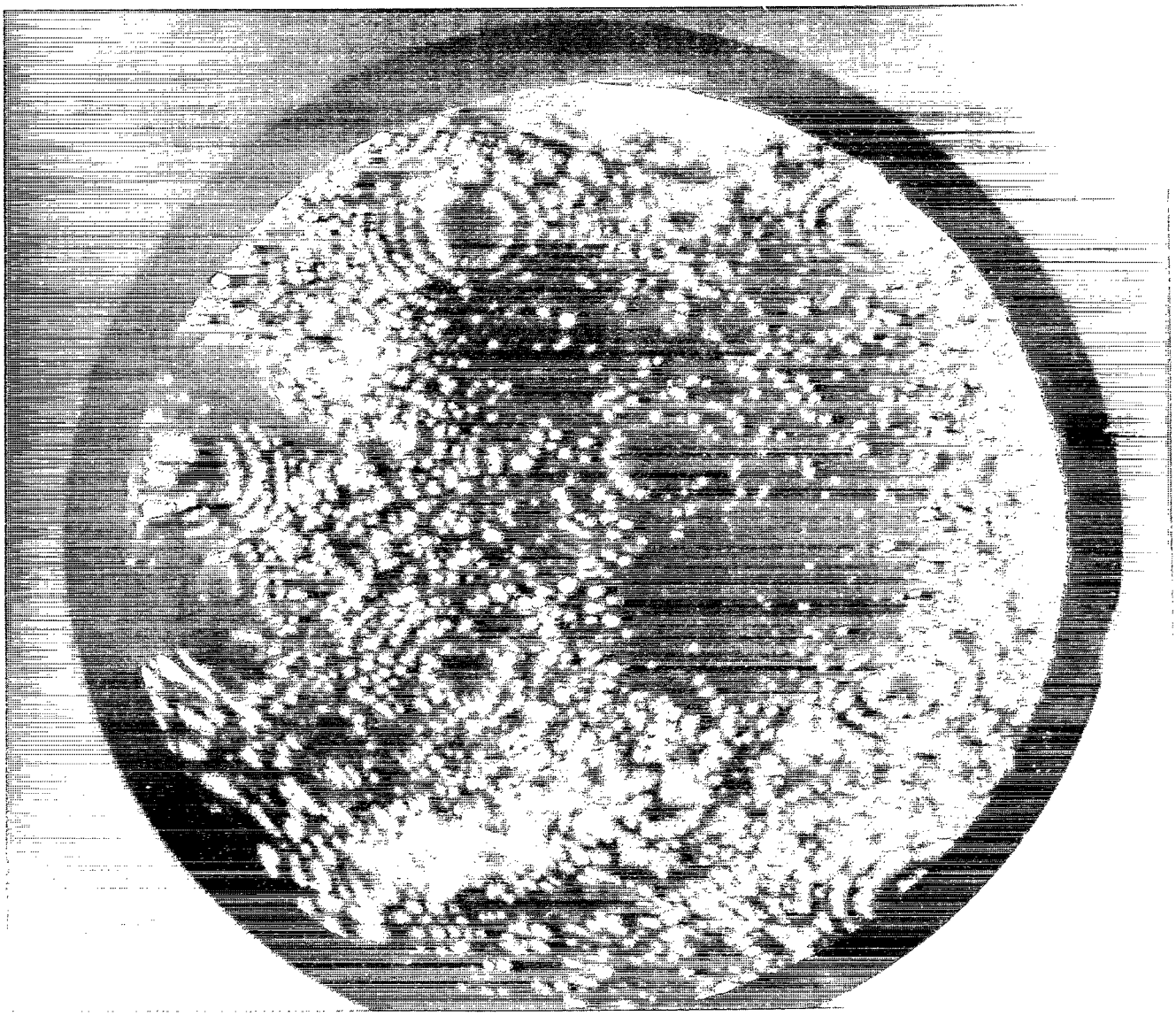

(c) Iridium after platinum contact at 19.0 kilovolts.

Figure 14. - Continued.

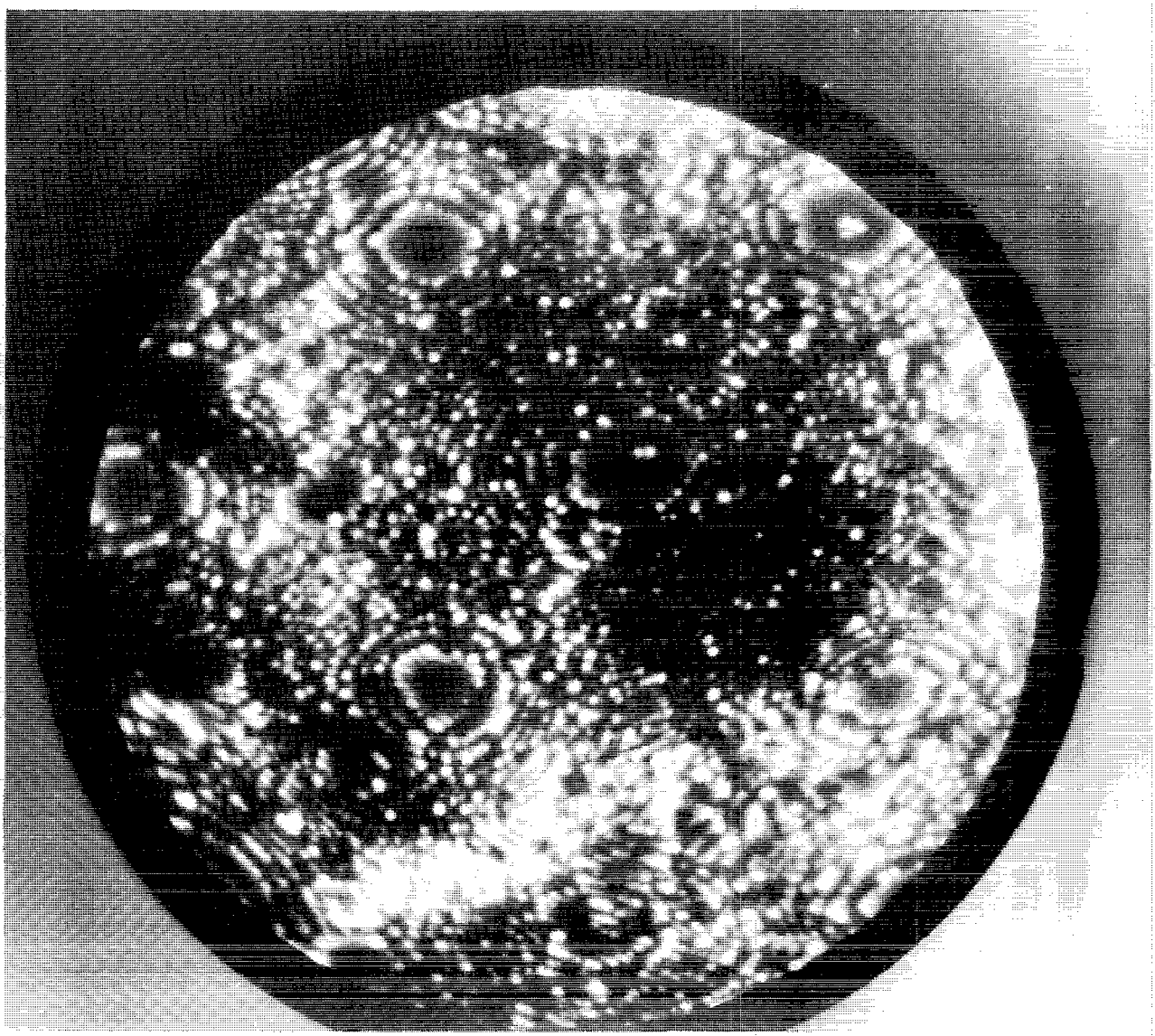

(d) Iridium after platinum contact at 20.0 kilovolts.

Figure 14. - Continued.

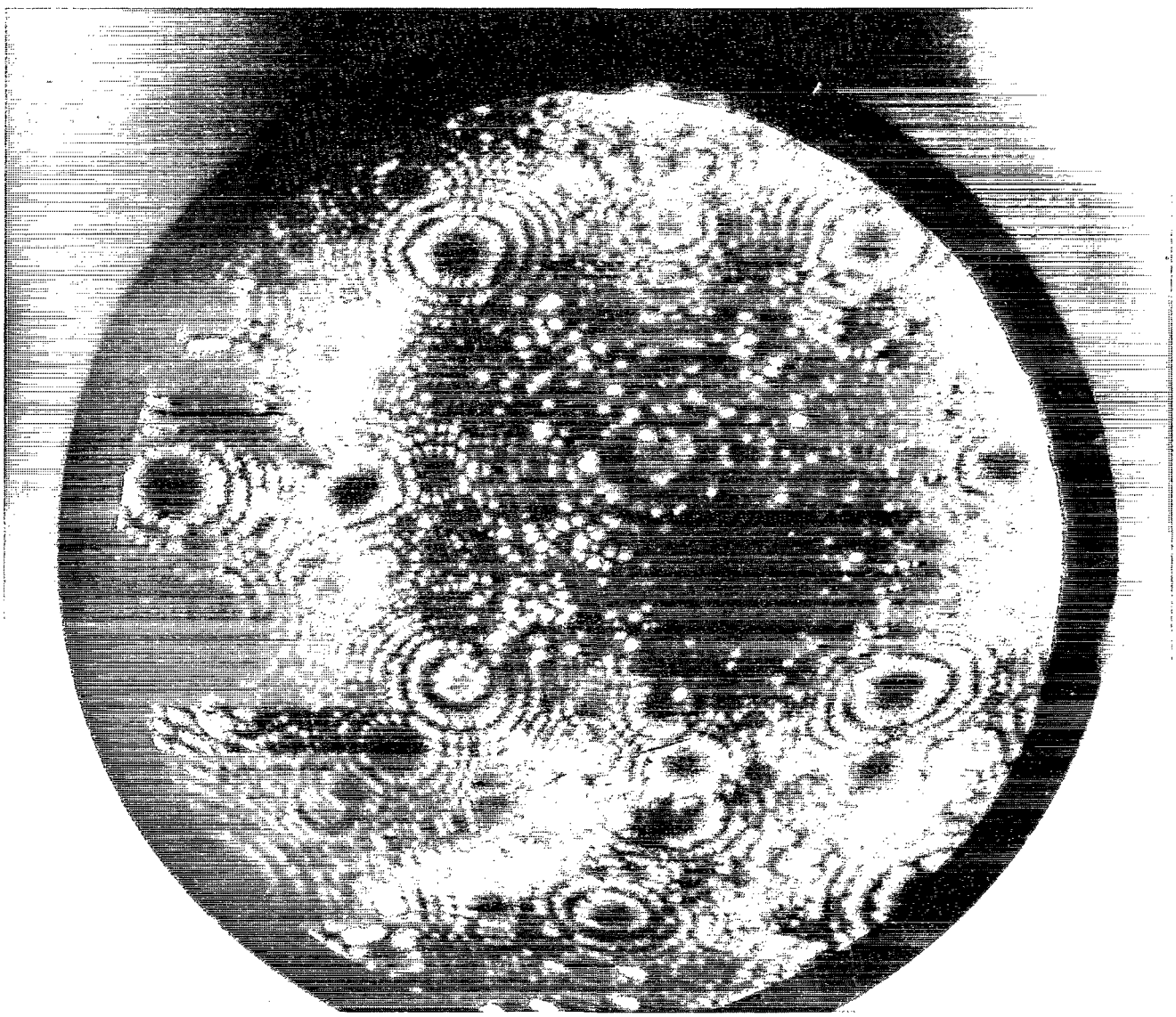

(e) Iridium after platinum contact at 20.0 kilovolts with voltage raised to 22.0 kilovolts for 30 seconds.

Figure 14. - Continued.

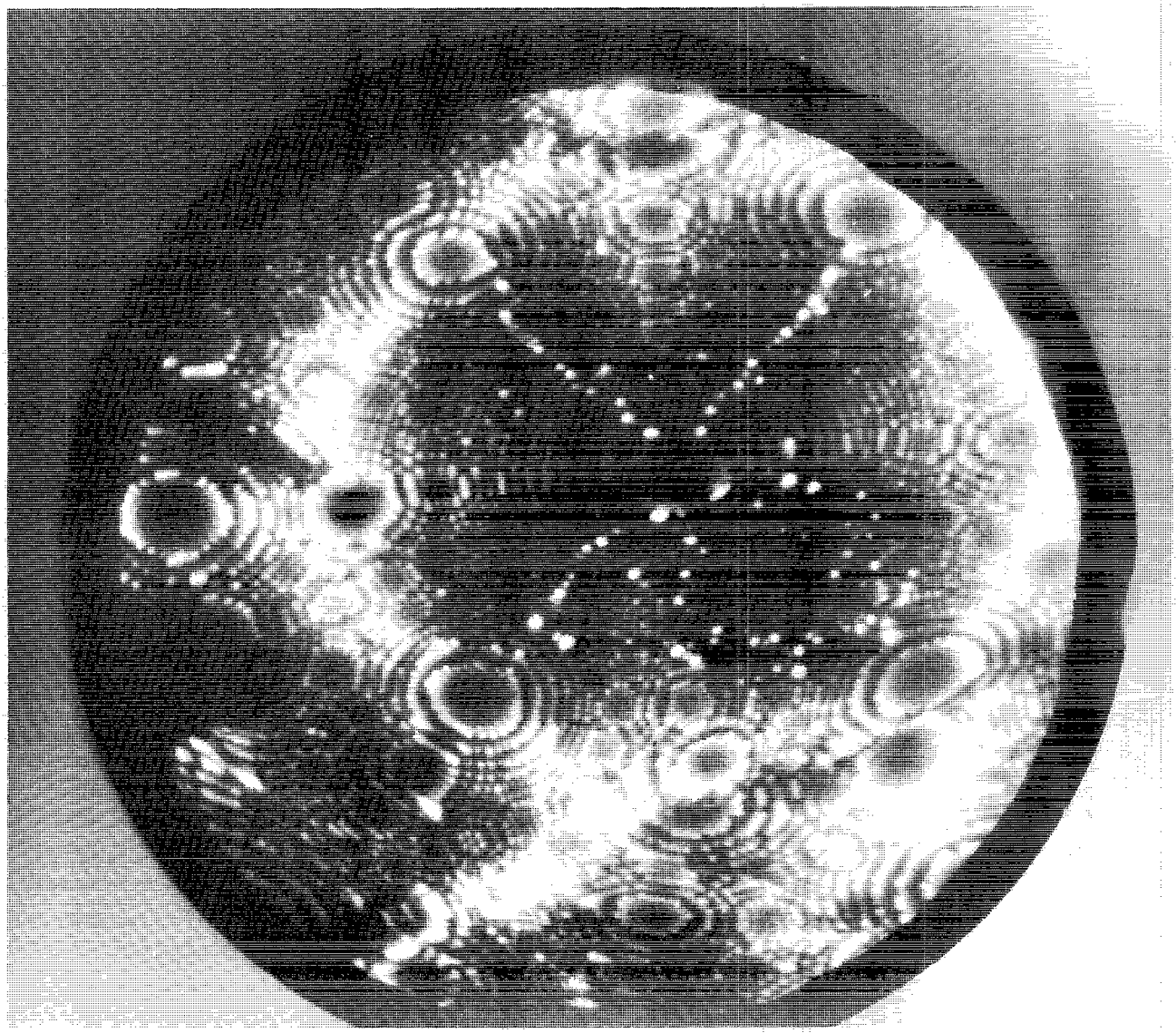

(f) Iridium after platinum contact at 20.0 kilovolts; two more (100) layers evaporated.

Figure 14. - Concluded.

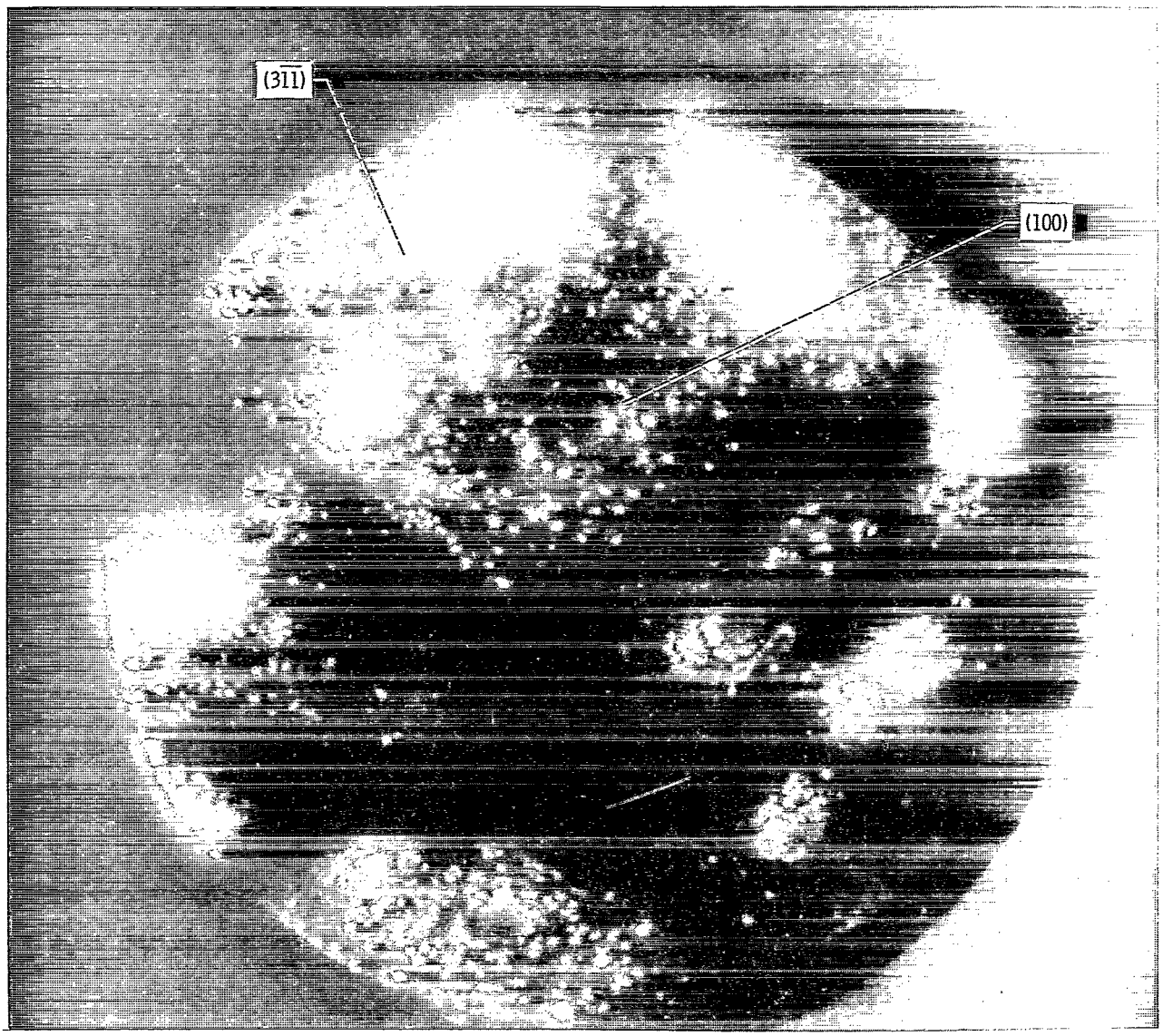

Figure 15. - Iridium after platinum contact at 28.0 kilovolts. No vibration isolation; image gas, helium; liquid-nitrogen cooling.

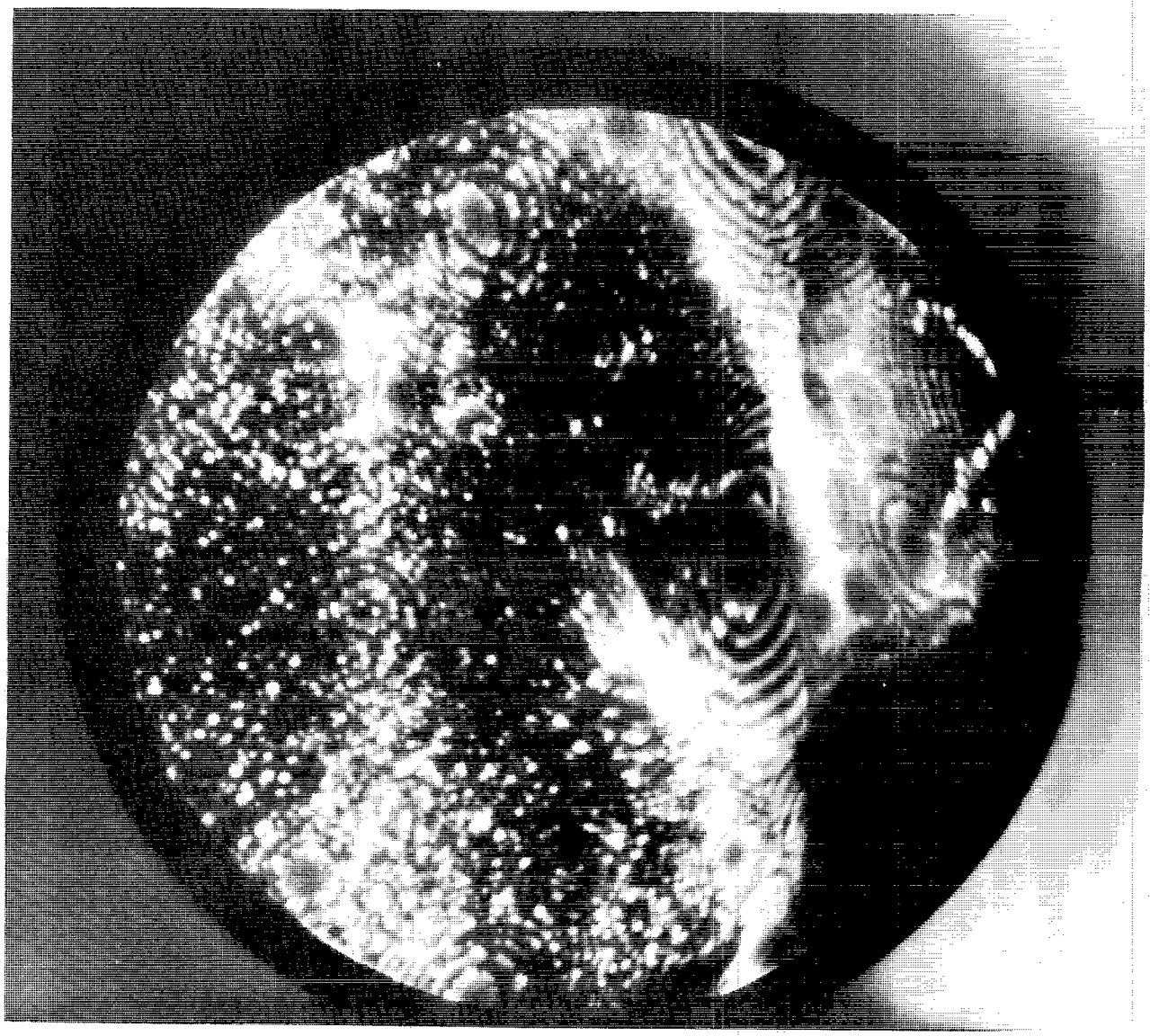

Figure 16. - Iridium after platinum contact with load of 1.3 to 1.5 milligrams at 23.0 kilovolts. Image gas, helium; liquid-nitrogen cooling.

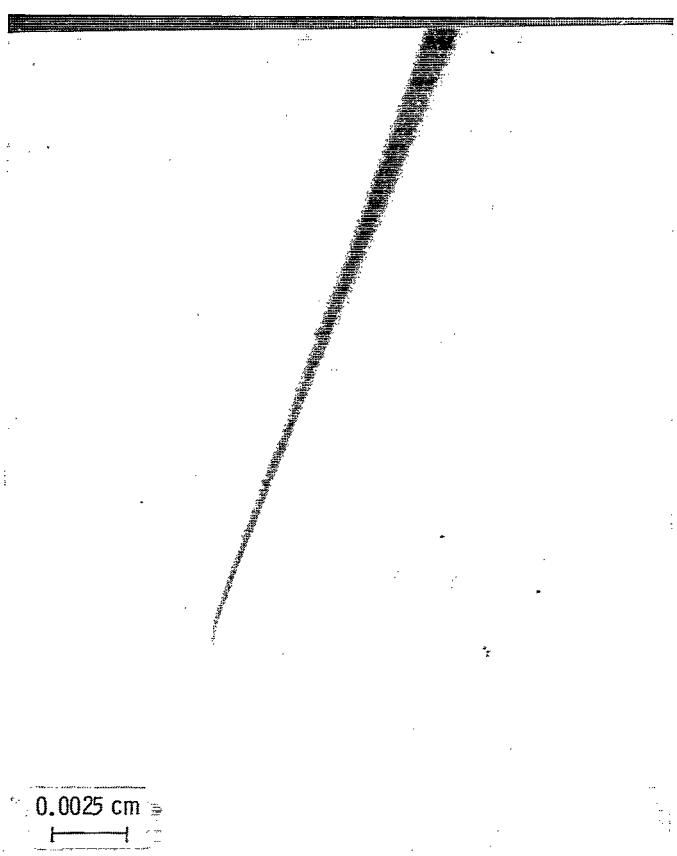

Figure 17. - Iridium tip after contact with platinum with a load of 1.3 to 1.5 milligrams.

NASA-Langley, 1971 —— 15 E-6383

"The aeronautical and space activities of the United States shall be conducted so as to contribute . . . to the expansion of human knowledge of phenomena in the atmosphere and space. The Administration shall provide for the widest practicable and appropriate dissemination of information concerning its activities and the results thereof."

—NATIONAL AERONAUTICS AND SPACE ACT OF 1958

NASA SCIENTIFIC AND TECHNICAL PUBLICATIONS

TECHNICAL REPORTS: Scientific and technical information considered important, complete, and a lasting contribution to existing knowledge.

TECHNICAL NOTES: Information less broad in scope but nevertheless of importance as a contribution to existing knowledge.

TECHNICAL MEMORANDUMS: Information receiving limited distribution because of preliminary data, security classification, or other reasons.

CONTRACTOR REPORTS: Scientific and technical information generated under a NASA contract or grant and considered an important contribution to existing knowledge.

TECHNICAL TRANSLATIONS: Information published in a foreign language considered to merit NASA distribution in English.

SPECIAL PUBLICATIONS: Information derived from or of value to NASA activities. Publications include conference proceedings, monographs, data compilations, handbooks, sourcebooks, and special bibliographies.

TECHNOLOGY UTILIZATION PUBLICATIONS: Information on technology used by NASA that may be of particular interest in commercial and other non-aerospace applications. Publications include Tech Briefs, Technology Utilization Reports and Technology Surveys.

Details on the availability of these publications may be obtained from:

SCIENTIFIC AND TECHNICAL INFORMATION OFFICE

NATIONAL AERONAUTICS AND SPACE ADMINISTRATION

Washington, D.C. 20546